SYNTHESIS OF SUPERBASE AND CORRELATION BETWEEN GAS PHASE ACIDITY AND pK_a STUDY OF IONIC LIQUID

by

PINGCHENG CHU

A thesis submitted to the

Graduate School-New Brunswick

Rutgers, The State University of New Jersey

For the degree of

Master of Science

Graduate Program in Chemistry and Chemical Biology

Written under the direction of

Professor Jeehiun K. Lee

And approved by

_____

_____

_____

_____

New Brunswick, New Jersey

[October, 2013]

ABSTRACT OF THE THESIS

SYNTHESIS OF SUPERBASE AND CORRELATION BETWEEN GAS PHASE ACIDITY AND pK_a STUDY OF IONIC LIQUID

By PINGCHENG CHU

Thesis Director:

Professor Jeehiun K. Lee

Since chemical reactions involving proton transfer as a key mechanism step become prevalent, development of Brønsted bases has been the intense focus in terms of catalyzing proton transfer reactions. Lambert *et al.* found and confirmed one cyclopropenimine as a strong superbase by measuring its pK_a in acetonitrile for the first time. Based on that, we calculated several cyclopropenimine's proton affinity (PA) which are much higher than all the volatile reference superbases we've ever

used. It means that if we could obtain those very basic superbases, they would be used as reference bases to bracket PAs of highly basic compounds. Herein, we tried to design and synthesize cyclopropenimine-based superbases and investigated their tunability of PA by modifying various electron withdrawing and donating groups. The corresponding calculation results are consistent with our proposal that cyclopropenimine superbase with EWG decrease PA while EDG increase PA. We also tried to measure PA of one cyclopropenimine superbase that we synthesized by Cooks kinetics method.

The other project focuses on a special class of ionic liquid which is known as green solvent with several advantages over traditional organic solvent. This new type of ionic liquid is imidazolium-based ionic liquid with tunable aryl and alkyl substituents which was designed by Strassner *et al.*. They named this category of ionic liquid as tunable aryl-alkyl ionic liquids (TAAILs). The reason we are interested in them is looking into the correlation between TAAILs' aqueous property and their theoretical acidity in gas phase and solution. If there was some correlation, we could predict imidazolium compounds' pK_a's by their gas phase property. Based upon this conjecture, we measured different TAAILs' acidity by LCQ bracketing method on mass spectrometry, calculated their free energy in solution phase as well as in gas phase and developed two methods to measure their pK_a's in solution. Their acidity

results demonstrate that those TAAILs with electron-withdrawing groups on para-position of phenyl substituent have high acidity while other TAAILs with electron-donating para-substituent have low acidity. Besides, I successfully obtained the pK_a value of one TAAILs as 25.4 in water via H/D exchange kinetics experiment on NMR.

ACKNOWLEDGEMENTS

During two years of study and research at Chemistry and Chemical Biology Department at Rutgers, I would like to give my sincere appreciation to my advisor, Dr. Jeehiun K. Lee, for all her guide, suggestions on my research work and words which would influence me to work better in the future. I would also like to thank Dr. Karsten Krogh-Jespersen and Dr. Warmuth, to be my committee members and their time in providing helpful advice on my experiments. Special thanks to Dr. Strassner in Germany for his collaboration on one project and Dr. Roger Jones and Dr. Seidel for allowing me using some experiment device in their labs.

I would like to thank the previous and current members of Lee group: Anna Michelson, Sisi Zhang, Landon Greene, Mu Chen, Kai Wang, Yuan Tian, Hao Zeng and Yijie Niu for their friendship and help in both my research and life.

Last, I am very grateful to the unending support and love from my parents and my friends. It is you who give me comfort whenever I am in trouble and aid me get through the tough time. You make me believe that I can still make it on my road in the future. I love all of you.

TABLE OF CONTENTS

LIST OF FIGURES

LIST OF TABLES

Chapter 1 Introduction

1.1 Overview

1.1.1 Proton affinity and gas phase acidity

The proton affinity (PA) of an anion or of a neutral atom or molecule is a measure of its gas-phase basicity.[1] The advantage of studying molecules' PA is that we can exclude the solvation effect in solution phase, and better understand their intrinsic properties. The definition of gas phase proton affinity (PA) is the negative enthalpy change of the protonation reaction, ranging from 130 to 291 kcal/mol [2](Eq. 1.1). The gas phase acidity is defined as the positive enthalpy change (ΔH_{acid}) of the deprotonation reaction (Eq. 1.2), ranging from 314 to 417 kcal/mol. The lower value of gas phase acidity corresponding to higher acidity, while the higher value of proton affinity corresponding to a higher basicity. In Chapter 2, we will describe the gas phase PA of a series of organic superbase with various substituents. In Chapter 3, we will focus on imidazolium-based ionic liquids by measuring their gas phase acidity and probe its correlation with acidity in solution.

$$HB^{+}_{(g)} \longrightarrow B_{(g)} + H^{+}_{(g)} \qquad \text{Eq. 1.1}$$

$$B_{(g)} + H^{+}_{(g)} \longrightarrow HB^{+}_{(g)} \qquad \text{Eq. 1.2}$$

1.1.2 Superbase

In chemistry, a superbase is an extremely strong base that is a compound with a high affinity for protons. Hydroxide ion is the strongest base possible in aqueous

solutions. However, since most reactions occur in organic solvents, therefore developing organic superbases is significant in organic synthesis and fundamental to physical organic chemistry. Organic superbases have also been defined semi-quantitatively as any species with a higher absolute proton affinity (PA = 245.3 kcal/mol) and intrinsic gas phase basicity (GB = 239 kcal/mol) than Alder's canonical proton sponge (1,8-bis-(dimethylamino)-naphthalene). So far, organic superbases based on phosphazene, amidine and guanidine moietis have PA ranging from 250 kcal/mol to 260 kcal/mol. More organic superbases with higher PA are in a bad need.

1.1.3 Gas phase proton affinity of Strassner carbene

Imidazolium-based carbenes are ligands of a variety of organometallic catalysts and with broad applications in organic synthesis[3-5], such as olefin metathesis and Mizoroki-Heck coupling. The protonated carbenes are ionic liquids which can be used as green solvent in organic synthesis[6]. Different from traditional construction of ionic liquids, imidazolium-based ionic liquid from Strassner *et al.* are tunable with the combination of sp^3 alkyl and sp^2 aryl substituents at the nitrogens of imidazolium core. The thermochemical properties of this class of carbenes and ionic liquids are barely explored, especially the gas phase proton affinity and acidity. We are interested in the proton affinity of carbenes (acidity of imidazolium cations) and trying to find the relation between proton affinity and their aqueous property.

1.2 Instrumentation

Electrospray ionization (ESI) is a technique used in mass spectrometry to produce ions. It transforms ions in solution into ions in the gas phase[7]. Many samples that previously were not suitable for mass analysis can be analyzed by the use of ESI. ESI can be used to analyze any polar compound that include adduct ions. In ESI, ions are produced and analyzed as follows:

1. The sample solution enters the ESI needle to which a high voltage is applied.
2. The ESI needle sprays the sample solution into a fine mist of droplets that are electrically charged at their surface.
3. The electrical charge density at the surface of the droplets increases as solvent evaporates from the droplets.
4. The electrical charge density at the surface of the droplets increases to a critical point, known as the Rayleigh stability limit. At this critical point, the droplets divide into smaller droplets because the electrostatic repulsion is greater than the surface tension. The process is repeated many times to form very small droplets.
5. From the very small, highly charged droplets, sample ions are ejected into the gas phase by electrostatic repulsion.
6. The sample ions enter the MS detector and are analyzed.

Figure 1.1 shows the steps in the formation of ions from highly charged droplets.

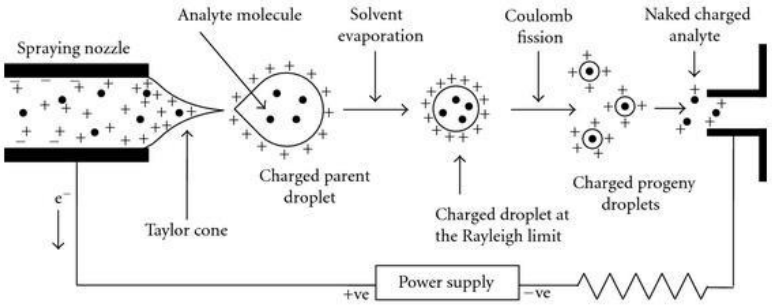

Figure 1.1 Electrospray ionization

The quadrupole ion trap is a highly sensitive and specific mass spectrometer component that consists of one ring electrodes and one entrance endcap electrode and one exit endcap electrode [8] (Figure 1.2). The inner surfaces of electrodes are hyperbolic. Together, they form a cavity in which mass analysis occurs. Ions are generated by ESI and then trapped, excited and ejected by the three hyperbolic electrodes cavity. A dc offset voltage, called the mass analyzer dc offset voltage, is applied to the mass analyzer electrodes to draw in ions from the ion optics. The magnitude of the mass analyzer dc offset voltage is -10 V for positive ion polarity mode and +10 V for negative ion polarity mode. Various ac voltages are applied to the ring and endcap electrodes to trap, fragment and eject ions according to their mass-to-charge ratios. Those ions move toward the center of ion trap, destabilize and eject by altering the amplitude of the ac[9].

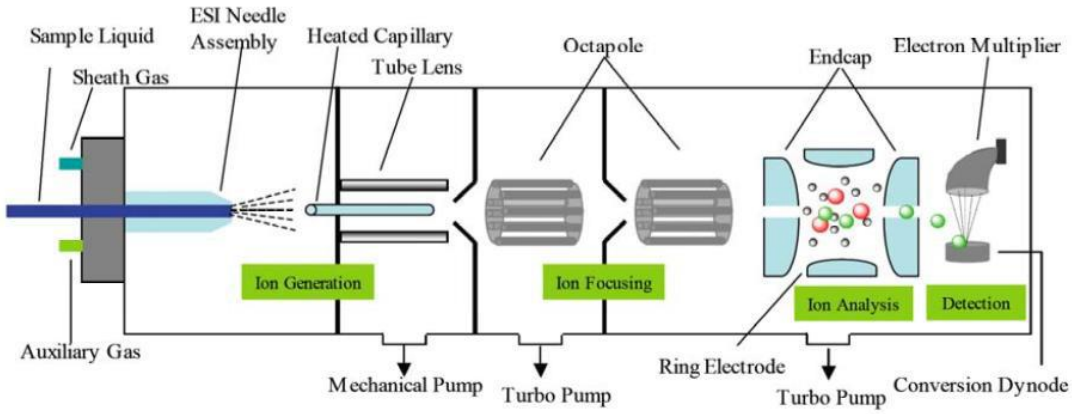

Figure 1.2 Schematic of a 3D ion trap mass spectrometer

1.3 Methodology

1.3.1 Bracketing method in LCQ

LCQ Bracketing method uses a series of reference bases to deprotonate the compound of interest, bracketing its proton affinity to a small range. Generally, reference bases are introduced into LCQ by vaporizing as neutral compounds. The studied compound is dissolved in the solvent which contains active protons (<100μM) and isolated as protonated compound to react with neutral references at different reaction time. The proton affinity of studied compound is determined by the protonation reaction occurring between compound anions and neutral references. If protonation reaction occurs, PA of compound is higher than that of reference base; while if there is no protonation reaction, PA of compound is lower than that of reference. The setup of LCQ bracketing method is illustrated in Figure 1.3.

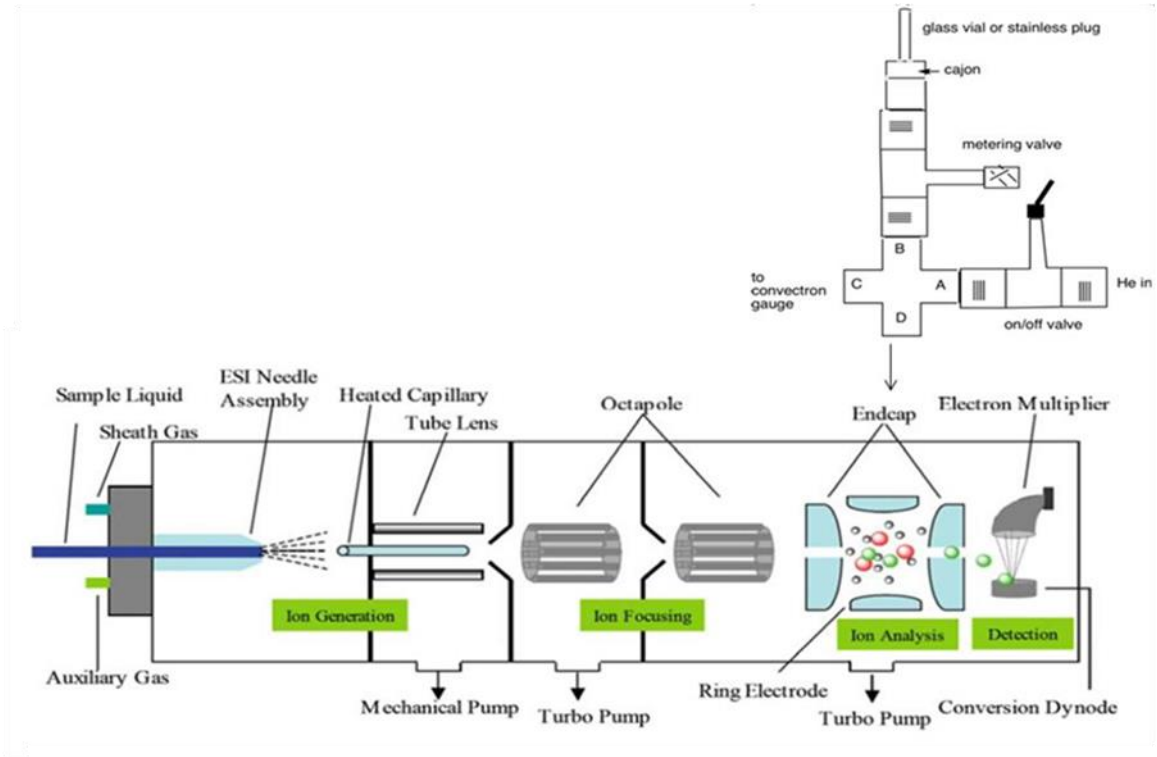

Figure 1.3 Schematic of LCQ bracketing experiments

1.3.2 Cooks Kinetic Method

The Cooks Kinetic Method was developed by Cooks and coworkers in the 1970s [10-13] . This approach uses kinetic information to study the thermochemical properties in the gas phase. Like what the figure 1.4 describes, AH^+ represents the compound with unknown acidity and B_iH^+ represents a series of reference acids.[14]

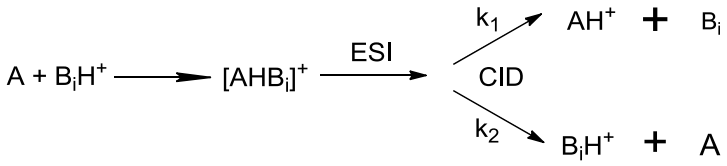

Figure 1.4 CID of proton-bound complex of acid and reference acids

In our experiments, the Cooks kinetic method was performed in a quadrupole ion trap mass spectrometer (Thermo Finnigan LCQ). Sample compound are mixed with reference acids in methanol or (dry) acetonitrile (with formic acid). The mixed solutions were ionized by electrospray ionization (ESI) and the proton-bound complex ions (dimers) were isolated and subjected to collision-induced dissociation (CID) in the ion trap analyzer. Therefore, Cooks kinetic method involves two competitive reactions, if compound A has a higher PA, the proton-bound dimer would be split into AH^+ and B, vice versa. The ratio of rate constants (k_1/k_2) of the two dissociation pathways is represented by the ratio of relative ion abundance of the AH^+/BH^+. Acidity of sample compound relative to the reference acids are calculated by Eq. 1.3. $\ln(k_1/k_2)$ was plotted versus the known acidity for a series of references, and the acidity of sample compounds can be obtained directly from the intercept of the resulting line.

$$B_iH^+ + A \overset{K}{\rightleftharpoons} AH^+ + B_i$$

$K \approx k_1/k_2 \sim$ relative ion abundance of the AH^+/B_iH^+

$$\ln(k_1/k_2) = \frac{1}{RT_{eff}}(PA(A) - PA(B_i)) \qquad \text{Eq. 1.3}$$

1.3.3 Calculations

Relative energies (gas phase acidities and proton affinities) of all compounds that we studied were calculated using the B3LYP method with 6-31+G(d) basis set in Gaussian 09[15] , and all the geometries were fully optimized at 298K. Modification of dihedral angles and conformation of cyclohexyl groups on cyclopropenimine-based superbases with various substituents were carried out on AM1 model. Solvation studies were conducted using the conductor-like polarizable continuum model (CPCM), where molecules were optimized at B3LYP/6-31+G(d) and UAKS radii are used [16, 17]. A dielectric constant of 78.3553 was used to simulate an aqueous environment in water as well as deuterated water. A dielectric constant of 35.688 was used to simulate an aqueous environment in acetonitrile.

Chapter 2 Superbase project

2.1 Introduction

This project is inspired by one of Prof. Lambert's publications *Enantioselective Brønsted Base Catalysis with Chiral Cyclopropenimines*[18], in which the basicity of a 2,3-bis(dialkylamino) cyclopropenimine (CPI) 1 is measured

for the first time with pK_{BH+} of 26.9 which is approximately equivalent to the pK_{BH+} 26.98 of tBu-P_1(dma) phosphazene, both considered as exceptionally strong bases(Figure 2.1)[19-21]. This finding classifies CPI 1 as a potent stong base.

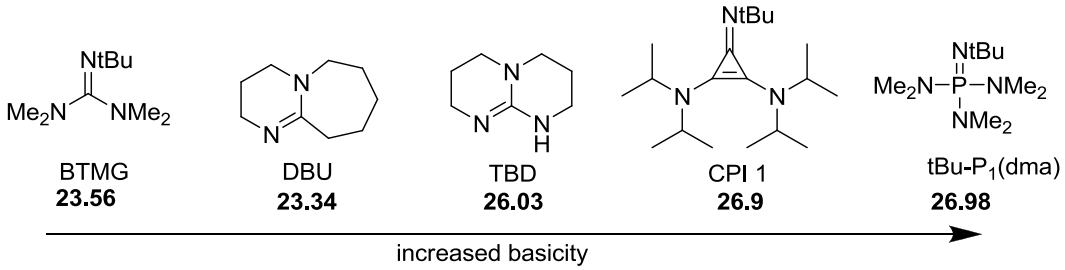

Figure 2.1 Basicity of cyclopropenimine 1 and several common strong organic bases. Bold numbers are pK_{BH+} values in acetonitrile

As we all know, since chemical reactions involving proton transfer as a key mechanism step become prevalent, development of organic bases have been the intense focus in term of catalyzing proton transfer reactions[22-24]. Generally, an organic base catalyst must possess strength of basicity properly tuned to the acidity of a given substrate. In this regard, strong, neutral organic bases such as DBU (diazabicycloundecene) or TMG (tetramethylguanidine) have proven highly useful as reagents or catalysts for numerous transformations[25]. However, the amidine and guanidine functional moiety upon which these reagents are built have inherent limitations of basicity. Even though stronger basicity can be realized with phosphazene[26] structures, yet novel Brønsted bases with strong and tunable basicity are always pursued to broaden the Brønsted base arsenal.

One major function of those bases is the ability to serve as reference bases in measuring proton affinity of other compounds via LCQ bracketing or Cooks kinetics method. The bases with high proton affinity are named as superbase. There are a lot of definitions of superbase. From semi-quantitative perspective, superbases are species with a higher proton affinity (PA = 245.3 kcal/mol) and intrinsic gas phase basicity (GB = 239 kcal/mol)[27]. So far, all the superbase we have to measure PA of other compounds are shown in Figure 2.2. If the superbases with higher PAs could be synthesized, that would effectively extend the reference base pool to bracket more compounds with high PA_{gas}. Fortunately, as mentioned in Prof. Lambert's publication, a novel structure—2,3-bis(dialkylamino) cyclopropenimines has been found as potential superbases. The reason of their high basicity lies in stability of the protonated form, the cyclopropenium ion. Since the smallest ring system that satisfies Huckel's rules, the 2π-electron cyclopropenium ion provides substantial aromatic resonance stabilization to the conjugate acid of the cyclopropenimine[28-30]. Thus, this additional stabilization renders 2,3-bis(dialkylamino) cyclopropenimines highly basic(Figure 2.3). Based on the scaffold, two cyclopropenimines with similar substituents are constructed (Figure 2.4). CPI 1 has already been characterized by the Lambert *et al.*, while CPI 6 is designed as a counterpart. Both of them have been synthesized to investigate their basicity as well as the further application in PA measurement.

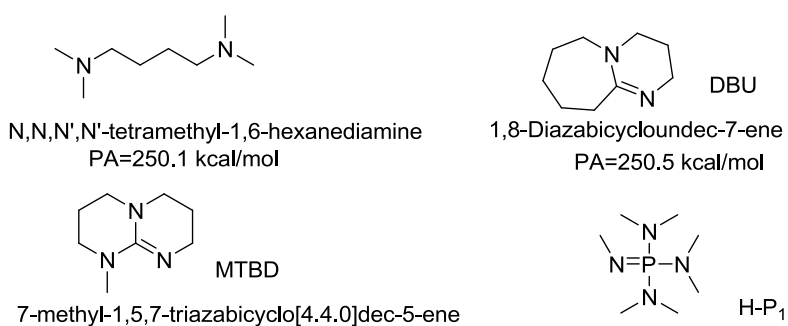

Figure 2.2 Common superbases available for LCQ bracketing or Cooks kinetic method

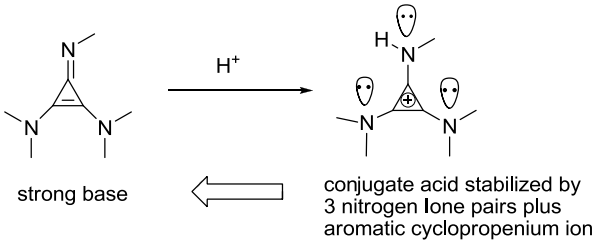

Figure 2.3 Cyclopropenimines as strong Bronsted bases

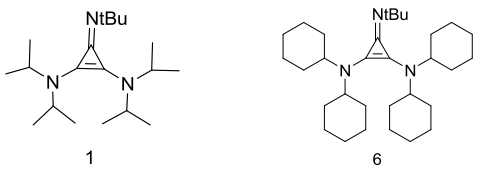

1 6

Figure 2.4 Structure of cyclopropenimine 1 and 6

2.2 Experiments and discussion

Chemicals diisopropylamine, perchloric acid, tert-butylamine, dicyclohexyl -amine, potassium tert-butoxide, dicyclohexylamine, tetrachlorocyclopropene, dichloromethane are commercially available except for monochlorocyclopropene cation which was synthesized following literature procedure[31]. Thin layer chromatography (TLC) was performed on silica gel 60 F254 plates (EMD). ^{1}H and ^{13}C NMR were recorded in $CDCl_3$ (unless otherwise noted) on Varian vnmrs 300 and 400 spectrometers as noted. Data for ^{1}H NMR are reported as follows: chemical shift(δ ppm), multiplicity (s=singlet, d=doublet, t=triplet, q=quartet, qt=quintet, m=multiplet), integration and assignment. Data for ^{13}C NMR are reported in terms of chemical shift.

Several routes have been proposed to synthesize CPI 1 and 6 (Scheme 2.1) The results demonstrate that either one-pot synthesis or step-by-step synthesis works well to produce the corresponding hydrochloride salt. All NMR spectra are shown in the Appendix. As for the last step, in the beginning, t-BuOK or NaOH were used to neutralize the hydrochloride salt 1 • HCl and 6 • HCl in CH_2Cl_2. However, after the ^{1}H-NMR (d-$CHCl_3$ as the solvent), ^{12}C-NMR (d-$CHCl_3$ as the solvent), MS (MeOH as the solvent) data were collected and analyzed, the products were finally untangled to be the ring-opening products* as shown in the Scheme 2.2. The mechanism of

ring-opening reaction is shown as below (Scheme 2.3). Since there is a considerable amount of water contained in CH_2Cl_2 plus the presence of base, the ring-opening reaction was induced. The t-BuOK base produces a large quantity of OH^- anion which undertakes the nucleophilic attack towards the imine.

Route-1 for compound 1

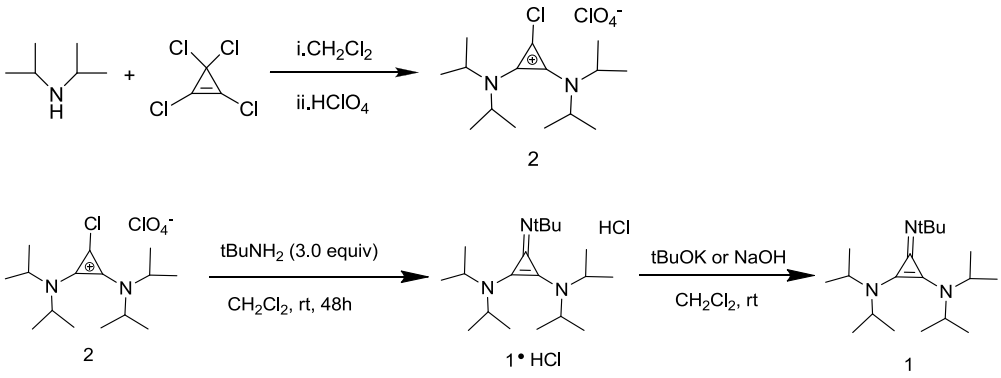

Route-2 for compound 1——one-pot synthesis

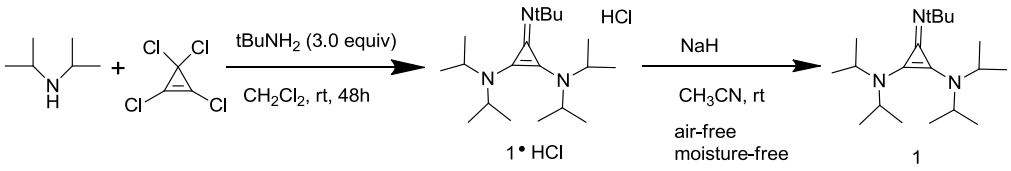

Route for compound 6——one-pot synthesis

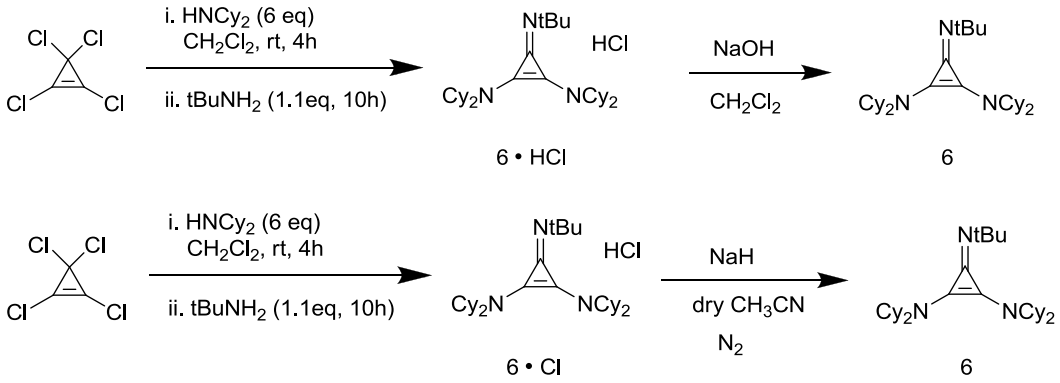

Scheme 2.1 Synthesis routes for compound 1 and compound 6

*Ring-opening reactions first observed by Lambert and Bandar, personal communication

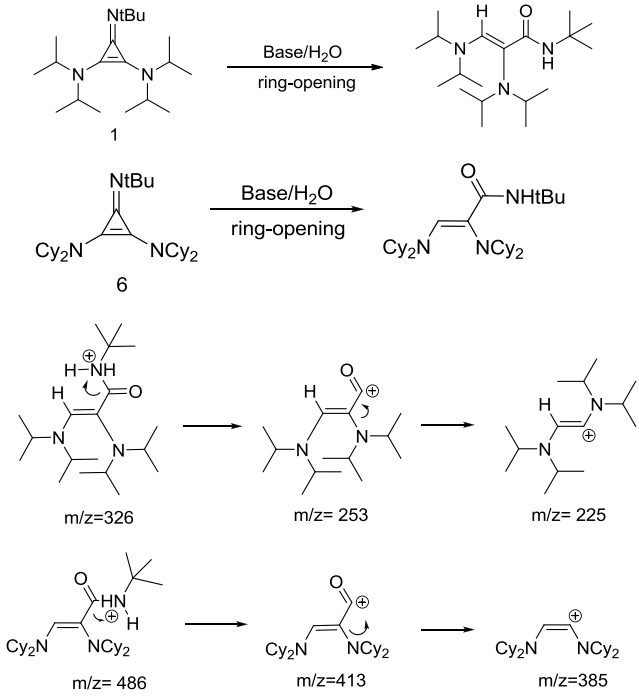

Scheme 2.2 The ring-opening side reactions and fragmentations and of compound 1 and compound 6

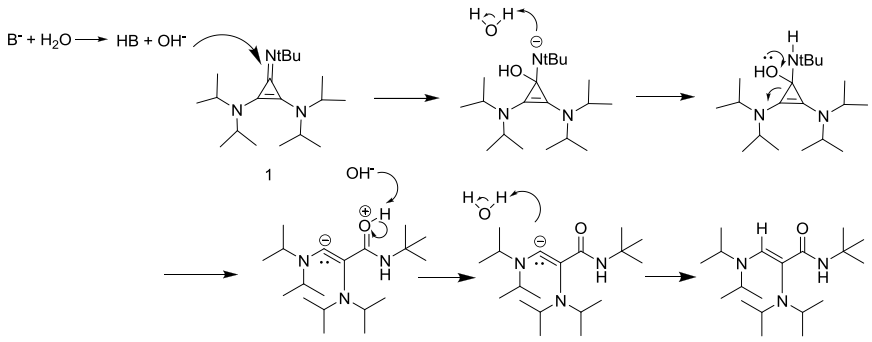

Scheme 2.3 Mechanism of ring-opening reaction

In order to eliminate the ring-opening reaction, the neutralization condition by using dry acetonitrile and N_2 atmosphere was optimized. The reaction was done twice by using NaH and t-BuOK as the base respectively. The combination of NMR spectra and MS spectra verify that the product is quite pure cyclopropenimine-1.

Even though the same moisture-free condition was also applied to neutralize cyclopropenimine-6 • HCl, somehow it still resulted to the ring-opening product. Another student in the lab also repeated the last step and failed neither. We came to a conclusion that cyclopropenimine-6 is more likely to undergo the ring-opening reaction.

2.3 Problem

However, the conclusion above is contradictory to three points of view in Prof. Lambert's paper, *Enantioselective Bronsted Base Catalysis with Chiral Cyclopropen -imines*. First, it is said that 2,3-bis(dialkylamino)-cyclopropenimines have ease of synthesis. The author developed a trivial large scale synthesis of compound 5 by the following route. (Scheme 2.4)

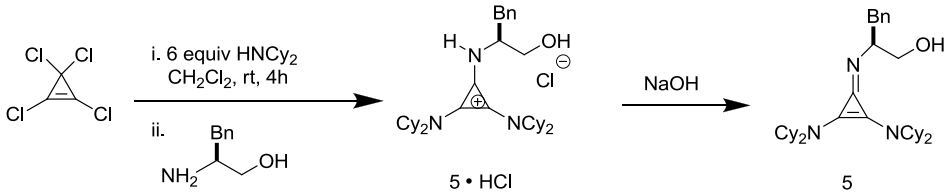

Scheme 2.4 synthesis route of cyclopropenimine 5

Second, the author announced that cyclopropenimine 5 is less basic than other cyclopropenimines. Based on the X-ray structure of the crystalline 5 ·HCl given (Figure 2.5), he attributed reason of less basicity to the presence of dicyclohexylamine

groups. The steric demand of the dicyclohexylamine groups causes these substituents to torque out of planarity with the cyclopropenium ring.

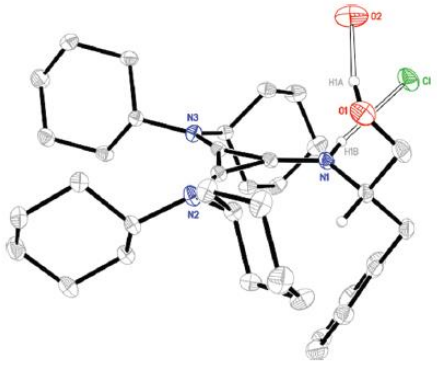

Figure 2.5 X-ray structure of the crystalline 5 ·HCl

Third, the author stated that cyclopropenimines differ greatly depending on what the amino groups are on the bottom of the cyclopropene. For example, the dicyclohexylamino imines are less basic than the diisopropyl imines, that is why NaOH can be used to depronate dicyclohexylamino CPI salt instead of the diisopropyl CPI salt. And the diisopropyl amino substituted imines seem to be much more sensitive to any wet conditions or protons. However, I failed in attempts to neutralize cyclopropenimine 6 by using NaOH even though it is also substituted by dicyclohexylamino groups.

2.4 PA_{gas} and ΔG_{sol} in acetonitrile calculation work

In order to figure out the relative basicity of the cyclopropenimines with different substituents, PA_{gas} and ΔG_{sol} in acetonitrile calculations have been accomplished.

To find the lowest point on the potential energy profile, altering the dihedral angle and conformation of cyclohexyl groups were used to optimize the enthalpy of those cyclopropenimines. Meanwhile we also calculated the ΔG of cyclopropenimines in acetonitrile by using CPCM method. $\Delta G_{sol}=G^0(A_{aq})+G^0(H^+_{gas})+\Delta G^0_s(H^+)-G^0(HA^+_{aq})$ where $G^0(H^+_{gas})$=-4.39kcal/mol, $\Delta G^0_s(H^+)$=-250.76kcal/mol in acetonitrile [32] The final calculation results are shown below in Figure 2.6.

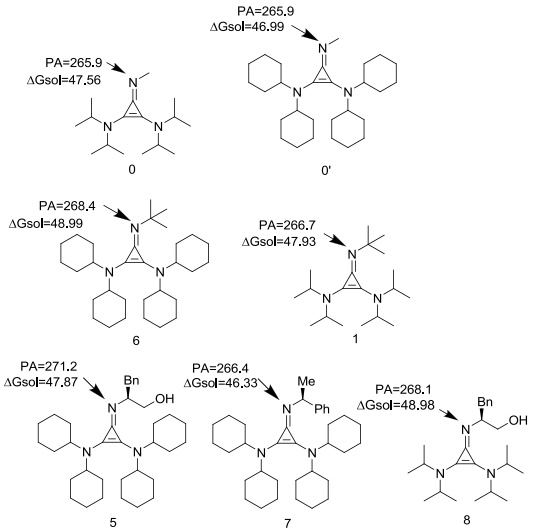

Figure 2.6 PA_{gas} and ΔG_{sol} in acetonitrile of cyclopropenimines by using B3LYP/6-31+G(d), CPCM, 298K, kcal/mol

It is worthy to notice that cyclopropenimine 5 and 8 have opposite trends in PA_{gas} and ΔG_{sol}. To investigate the discrepancy, gas-phase basicity was calculated for

these two cyclopropenimines by using free energy values and the corresponding potential energy profiles were also drawn out(Figure 2.7). GB=G(B)+G(H^+)$_{gas}$-G(BH^+) where G(H^+)= -4.39 kcal/mol [32]. From those potential energy profiles, it seems that the difference of ΔG_{solv} for neutral species is 5 kcal/mol more than that for ΔG_{solv} for protonated species.

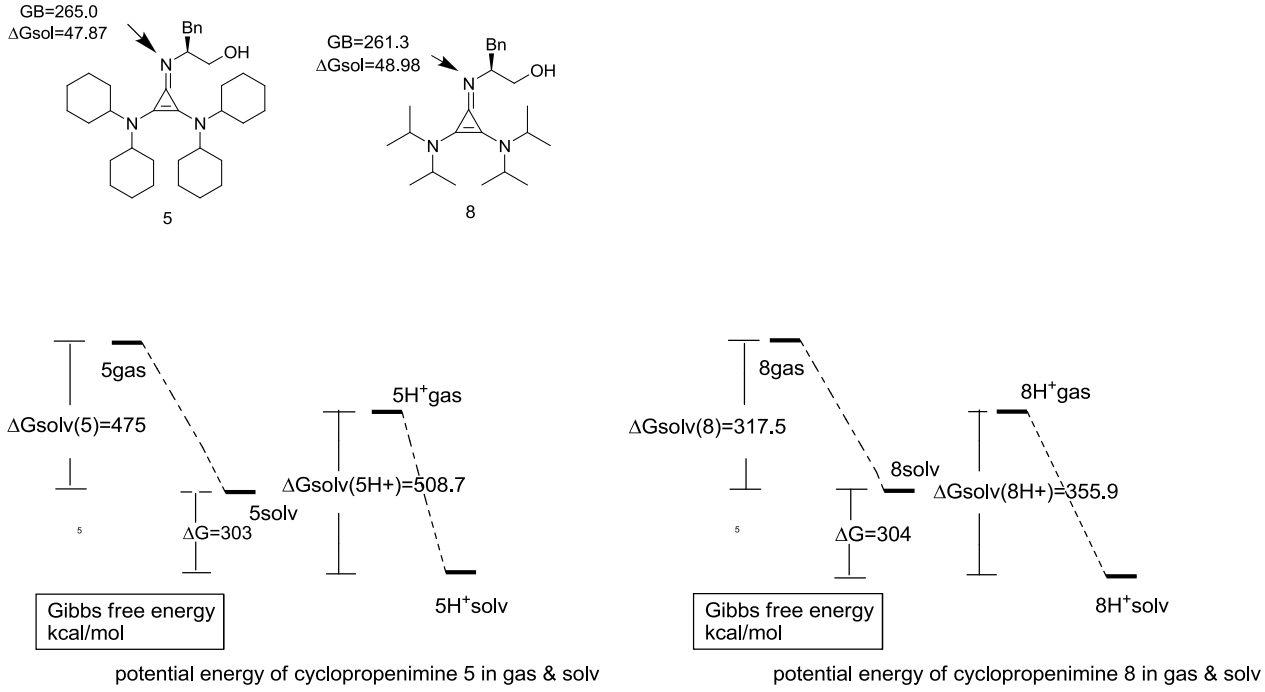

Figure 2.7 GB, ΔG_{sol} and potential energy of cyclopropenimine 5 and 8
$\Delta G_{solv}(5)-\Delta G_{solv}(8)$=158 kcal/mol $\Delta G_{solv}(5H^+)-\Delta G_{solv}(8H^+)$=153 kcal/mol

As comparison, the same work has done to cyclopropenimine 1 and 6. Gas-phase basicity was calculated for these two cyclopropenimines by using free energy values. GB=G(B)+G(H^+)$_{gas}$-G(BH^+) where G(H^+)= -4.39 kcal/mol [32]. From

the potential energy profiles (Figure 2.8), the difference of ΔG_{solv} for neutral species is almost the same with that for protonated species. Therefore, the trend in GB of the two compounds is parallel with the trend in their ΔG_{sol}.

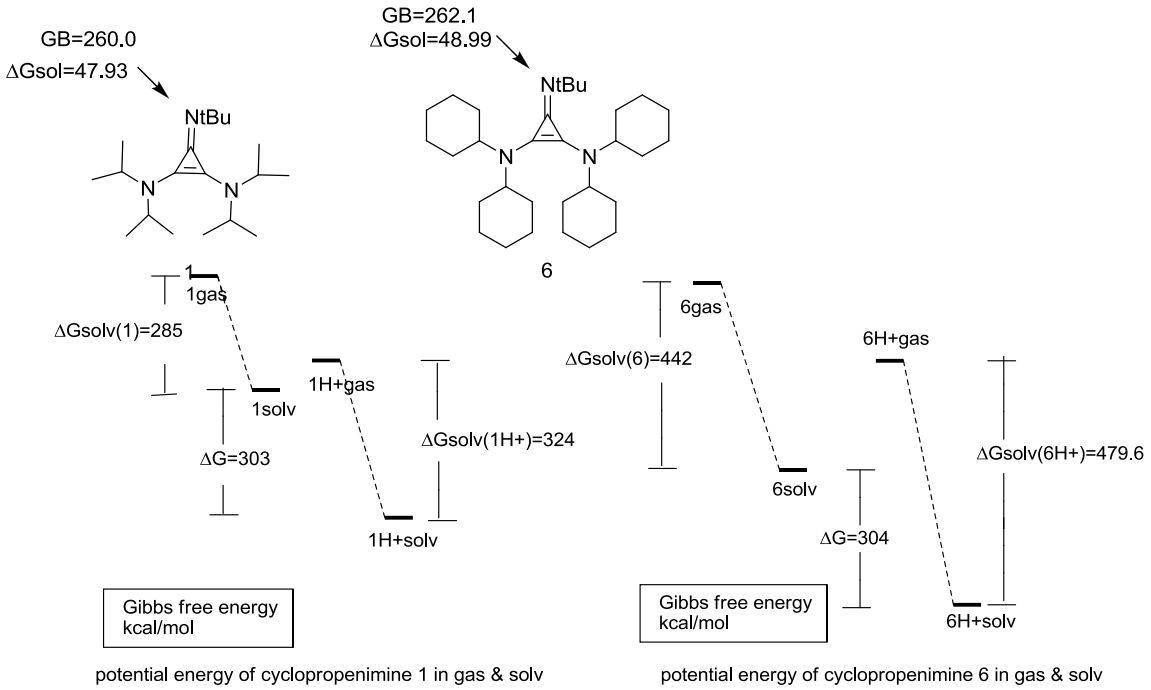

Figure 2.8 GB, ΔG_{sol} and potential energy of cyclopropenimine 1 and 6
$\Delta G_{solv}(6)-\Delta G_{solv}(1)=157$ kcal/mol $\Delta G_{solv}(6H^+)-\Delta G_{solv}(1H^+)=155.6$ kcal/mol

Based on the analysis above, Prof. Lambert's general statement that CPIs with dicyclohexylamine are less basic than the CPIs with diisopropylamine is not always true.

2.5 Cooks kinetic method for PA measurement

We tried Cooks kinetics method of cyclopropenimine-1 (M.W=307, PA=266.7) with five reference bases in dry acetonitrile on MS. (Figure 2.9)

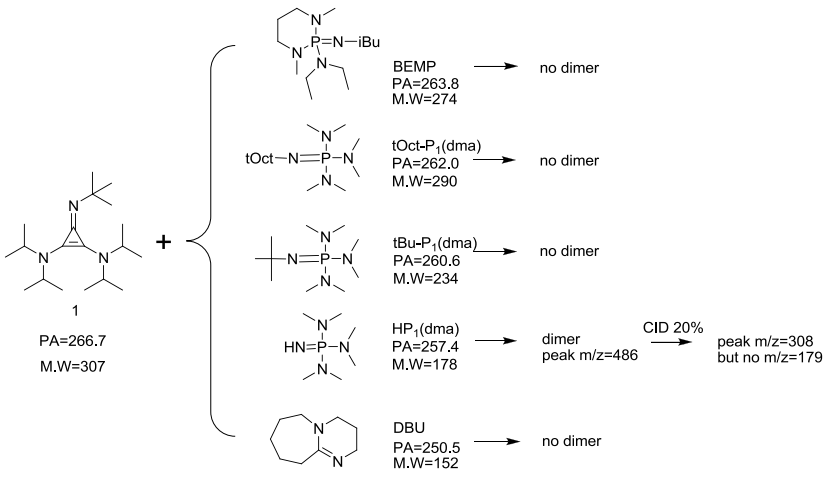

Figure 2.9 Cooks kinetics method of cyclopropenimine 1 with reference bases

No ring-opening product was observed after cyclopropenimine-1 was dissolved in dry acetonitrile with reference bases except for BEMP. There is dimer (the peak of m/z=486) formed when cyclopropenimine-1 reacts with HP_1(dma), but after being applied with CID ~20% to peak of m/z=486, only 308 peak (cyclopropenimine-1H^+) was observed. The result demonstrates that dimer can be formed between HP_1(dma) and cyclopropenimine-1, but their basicity gap is so large that the fragment of HP_1(dma) could not be observed after the dimer is collided. Therefore, some more cyclopropenimines to be tested by Cooks kinetics method are needed.

2.7 Tunability of substituents research

Before starting with synthesizing more other CPIs, it would be better for us to study the reaction mechanism, figuring out how we could modify the substituents. (Scheme 2.5)

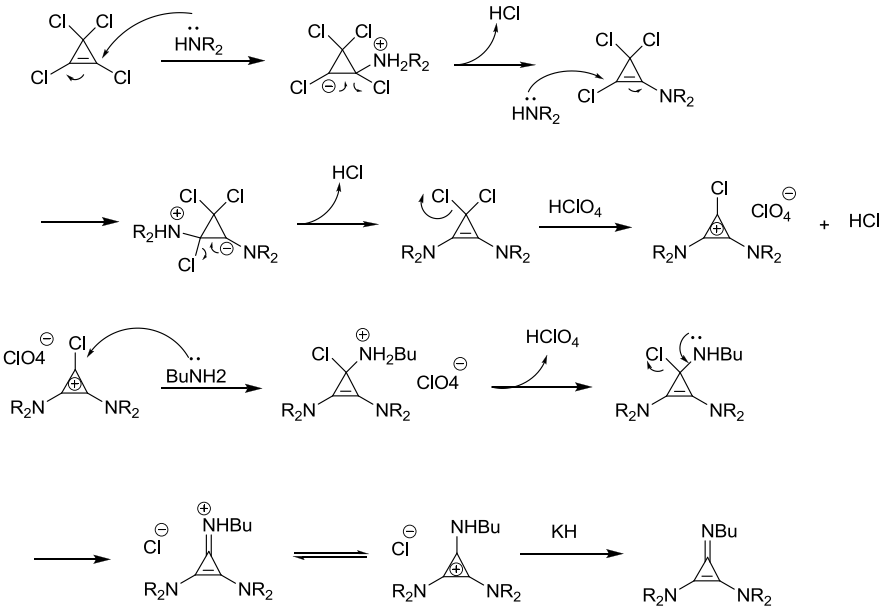

Scheme 2.5 Reaction mechanism of formation of cyclopropenimines

After studying the reaction mechanism, two aspects need to be considered in terms of the feasibility of adding upper substituent or bottom substituents. They are electrophilicity of the substrate and nucleophilicity of the substituents. The trends are shown as below.

Electrophilicity: 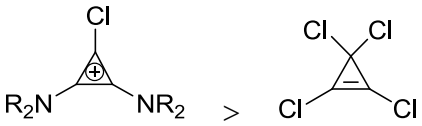

Nucleophilicity & Bulky sterics: 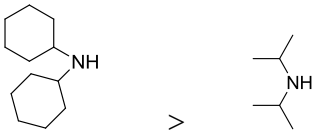

This trend demonstrates that the upper amine substituents are easier to be added onto the cyclopropenium ring than the bottom amine groups. Next up, we headed to investigate how electron-withdrawing group would influence the basicity of the cyclopropenimines. Herein, several cyclopropenimines with fluoro, cyano and carbonyl groups were constructed and their PA_{gas} were calculated. (Figure 2.10) It is

found that those EWGs dramatically decrease the PA_{gas} of cyclopropenimines which makes those cyclopropenimines less valuable as reference base with high PA_{gas}.

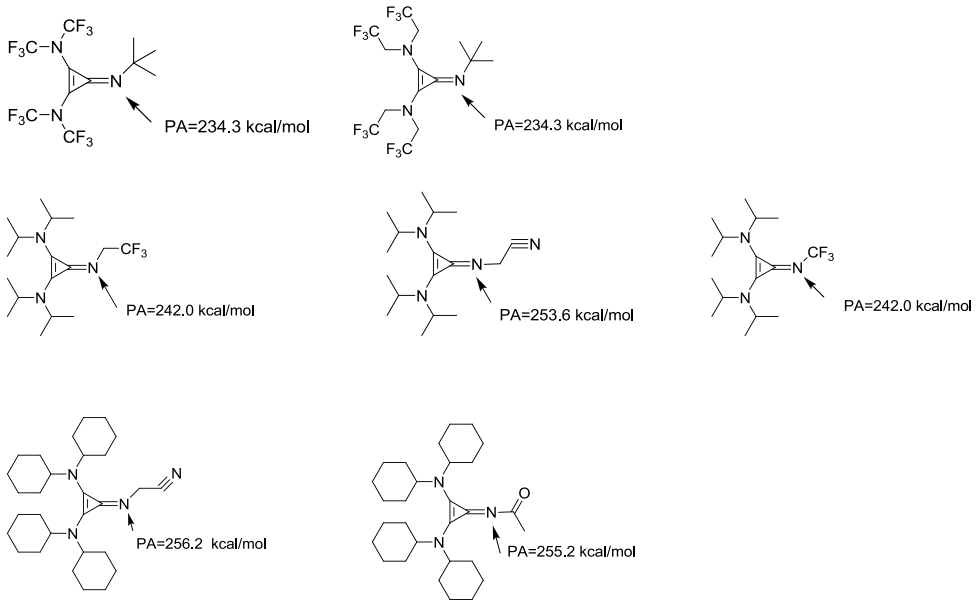

Figure 2.10PA_{gas} of different cyclopropenimines with EWG calculated by B3LYP/6-31+G(d), 298K, kcal/mol

Likewise, the cyclopropenimines with various EDGs were modified to see how the PA_{gas} would be influenced mildly. Their corresponding calculated PA_{gas} are shown below. (Figure 2.11) Obviously, those EDGs dramatically increase the PA_{gas} of cyclopropenimines which make those cyclopropenimines more valuable as reference base with high PA_{gas}.

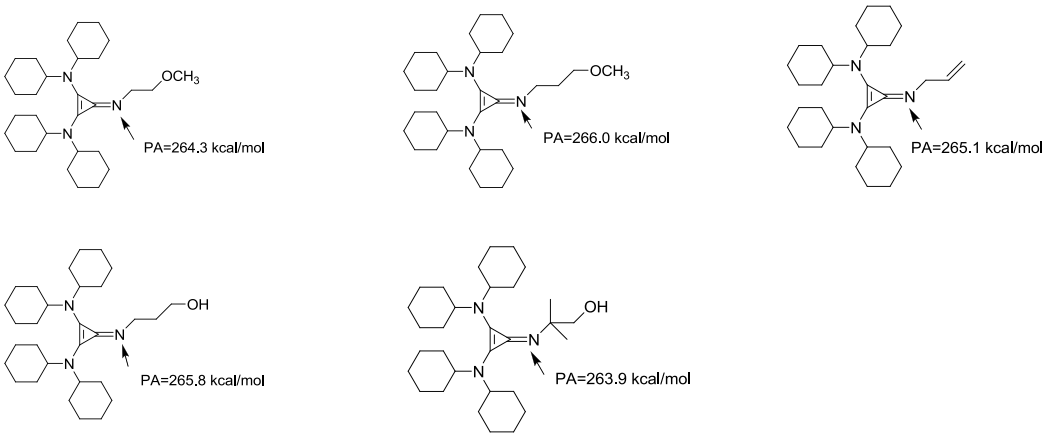

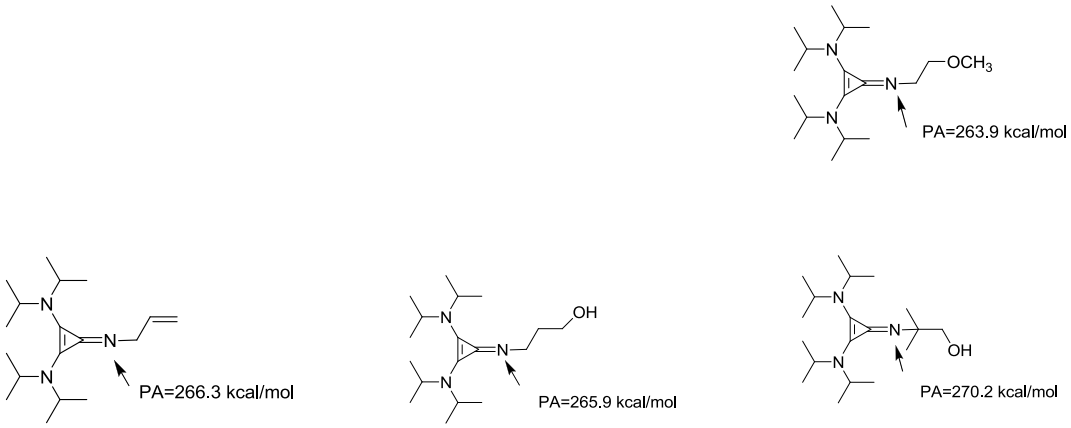

Figure 2.11 PA_{gas} of cyclopropenimines with various EDG calculated by using B3LYP/6-31+G(d) ,298K ,kcal/mol

Meanwhile, according to SciFinder, the synthesis of cyclopropenimines reported so far includes several structures below[33]. The corresponding PA_{gas} have been calculated. (Figure 2.12)

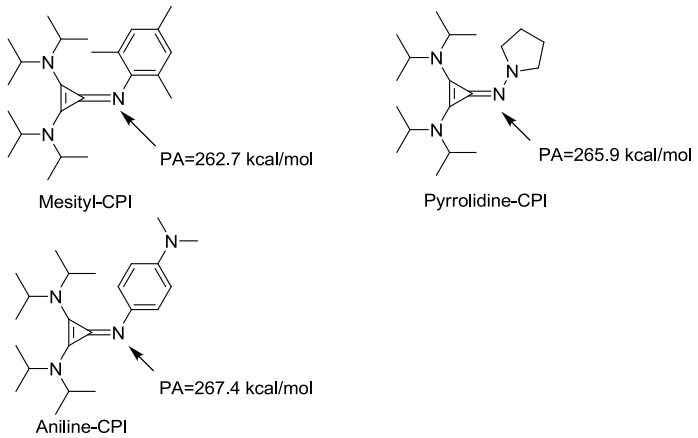

Figure 2.12 PA_{gas} of cyclopropenimines synthesized so far calculated by using B3LYP/6-31+G(d), 298K, kcal/mol

Inspired by the calculation above relating the phenyl-substituted cyclopropenimines, cyclopropenimines substituted by phenyl with various electron-withdrawing groups at para position are conceived and the corresponding PA_{gas} have been calculated. (Figure 2.13)

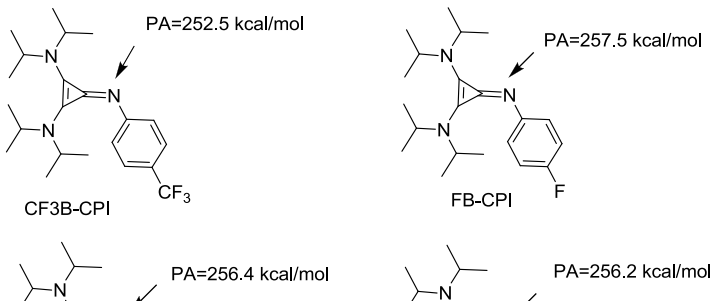

Figure 2.13 PA_{gas} of cyclopropenimines with phenyl group calculated by using B3LYP/6-31+G(d),298K, kcal/mol

2.8 Conclusion

So far, in this project, we had synthesized successfully cyclopropenimine-1 but not cyclopropenimine-6, even though the same neutralization condition was applied to deprotonate the CPI-6 •HCl. We came to the initial conclusion that CPI-6 is more likely to ring-open which is contradictory with Lambert's statement that cyclopropenimine with dicyclohexylamine are less basic than the CPIs with diisopropylamine. After further research by calculating thermochemical property, such as GB and ΔG_{sol} of pairs of CPIs with dicyclohexylamine and diisopropylamine, we found that CPIs with dicyclohexylamine is not always less basic than CPIs with diisopropylamine. Then, in order to investigate how those substituents effect basicity, we constructed various CPIs by modified their substituents after we studied the mechanism behind cyclopropenimine's synthesis reaction. The calculation results of those CPIs confirm that EDGs dramatically increase the PA_{gas} of cyclopropenimines while EWGs decline. Considering the difficulty involved in synthesizing CPIs with

higher PA, we are interested in CPIs with moderate basicity which might be realized by constructing EWGs on para-site of phenyl ring connected with imine. The calculation results show that most of their PAs between 255-260 kcal/mol.

2.9 Proposed Research

Based on all data obtained above, we need to synthesize more cyclopropenimines to be applied as reference bases in LCQ bracketing or Cooks kinetics method. Among those cyclopropenimines, Mesityl-CPI (PA_{calc}=262.7 kcal/mol), CF_3B-CPI (PA_{calc}=252.5 kcal/mol), ClB-CPI (PA_{calc}= 256.4 kcal/mol), BrB-CPI (PA_{calc}= 256.2 kcal/mol) are good candidates for the useful superbases, the synthesis process can take that on the literature [33]as reference (Scheme 2.6). If those compounds could be successfully bracketed, they would be functioned as reference base to measure PA_{gas} of other compounds in the future.

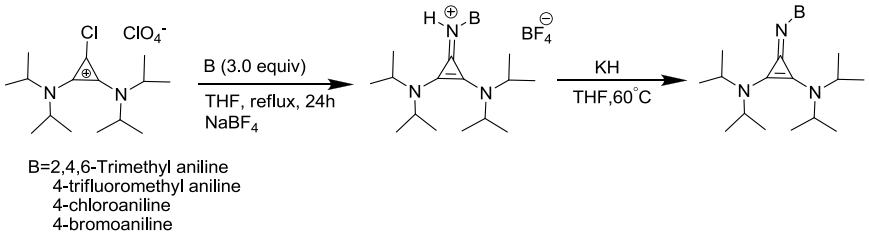

Scheme 2.6 The synthesis routes from literature [33]

Chapter 3 Strassner carbene project

3.1 Introduction

Ionic liquid (IL) which is well known as “green solvent” with several advantages over traditional organic solvent has recently received a lot of attention as alternative solvent for organic synthesis. Several classes of ionic liquids based on different organic cations have been investigated throughout the past years. ILs with imidazolium cation have become the most prominient to be used to design room-temperature ionic liquids. However, the properties of imidazolium-based salt are restricted by the alkyl chains on nitrogen.

To obtain a greater variation of ionic liquids’ properties, Strassner *et al.* designed a series of ionic liquids with the combination of sp^3 alkyl and sp^2 aryl substituent at the nitrogen of imidazolium core. The properties of this type aryl-alkyl ionic liquid are tunable by varying aryl substituent, so Strassner *et al.* termed it as tunable aryl-alkyl ionic liquids (TAAILs) (Figure 3.1)[6]. TAAILs can not only be tuned by Van der Waals interations, but also by π-π interactions between aryl group and imidazolium core.

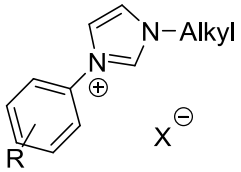

Figure 3.1 Tunable aryl-alkyl ionic liquid (TAAILs)

Strassner *et al.* pointed out that the melting point of this new type of ionic liquid is tunable by changing the (para-) aryl substituents. However, no one has ever investigated the other fundamental properties of TAAILs. Therefore, we are interested in probing the acidities of TAAILs, which will aid people to understand and use this new type of ionic liquid better in the future. On the other hand, since experimental pK_a's of those ionic liquids are not easy to be measured while PA_{gas} or PA_{sol} of those compounds are facile to obtain by calculation. If possible, a valid rationale could be established to correlate pK_a and PA_{gas} for similar carbenes. The method is valuable in predicating those pK_a's of some carbenes whose experimental aqueous acidity are not easily measured.

In order to verify the potential correlation between pK_a and gas phase acidity, we develop two approaches to measure pK_a. One is based on thermodynamics acidity in which chemical shift change is detected by NMR when the substrate is deprotonated by base. The other is established on kinetics acidity in which integration change of the carbene proton is monitored by NMR when it is subjected to H/D exchange reaction[34]. Below is the detailed explanation of this method.

According to Tina L. Amyes' literature *Formation and Stability of N-Heterocyclic Carbenes in Water: The Carbon Acid pK_a of Imidazolium Cations in*

Aqueous Solution[31], investigating the second-order rate constants k_{DO} ($M^{-1}s^{-1}$) for the deuterium exchange reactions of imidazolium cations to give the corresponding singlet carbenes at 25 ℃ and I = 1.0 (KCl) is used to obtain pK_a as long as no hydrolysis or formation of dimer for those imidazolium during deuterium exchange. [35-38]

The procedure of the deuterium exchange reaction is shown in Scheme 3.1

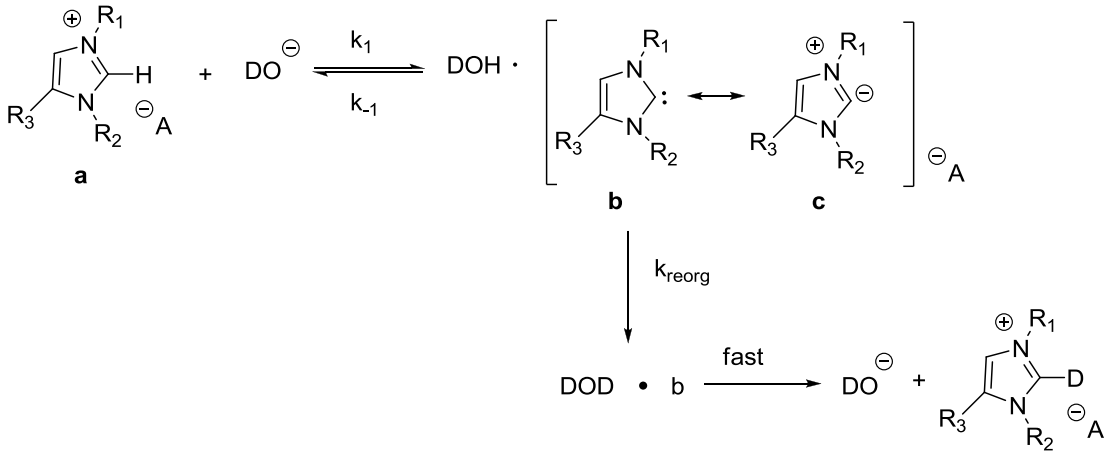

Scheme 3.1 Deuterium exchange reaction of imidazolium

Imidazolium ions are deprotonated by a base in D_2O solution to form carbene **a**, which is more appropriately represented by an ylidic resonance structure **c**. Solvent reorganization then occurs, which involves replacement of HOD by a DOD molecule. At typical substrate concentrations (5-10 mM), the concentration of the protonated

DOH is much smaller relative to that of bulk D_2O solvent. Thus reprotonation of the carbene by DOH to generate the protonated substrate is negligible and effectively irreversible.[25]

The fraction of substrate remaining f(s), for imidazolium ions **a** is determined from Equation 3.1

$$f(s) = \frac{(A_{C2-H} / A_{Std})_t}{(A_{C2-H} / A_{Std})_{t=0}} \qquad \text{Equation 3.1}$$

"A" represents the integration area of the corresponding peak in ^{1}H NMR spectra

The observed pseudo-first-order rate constant for exchange of the C2-H of **a** for deuterium is then determined from semi-logarithmic plots of f(s) against time (Equation 3.2).

$$\ln f(s) = -k_{obs}t \qquad \text{Equation 3.2}$$

The concentration of deuterioxide ion could be calculated using Equation 3.2, where $K_w = 10^{-14.87}$ M^2 is the ion product of D_2O at 25 ℃. A value for the apparent activity coefficient of deuterioxide ion, γ_{DO}, could be determined under experimental conditions of ionic strength 1.0 maintained with KCl.

$$[DO^-] = \frac{10^{pD-pKw}}{\gamma_{DO}} \qquad \text{Equation 3.3}$$

Then it comes to the determination of second-order rate constants for deuterioxide ion-catalyzed exchange k_{DO} ($M^{-1}s^{-1}$).The observed experimental pseudo-first-order rate constant for exchange (k_{obs}) is the sum of the contributions of all potential catalytic species to the exchange reaction, including contributions by solvent (k_{D2O}), deuterioxide ($k_{DO}[DO^-]$), and buffer base ($k_B[B]$) (Equation 3.4).[39]

$$k_{obs} = k_{D2O} + k_{DO}[DO^-] + k_B[B] \qquad \text{Equation 3.4}$$

The equation 3.4 could be abbreviated as equation 3.5 since the buffer base catalyst is negligible.[40]

$$k_{obs} = k_{D2O} + k_{DO}[DO^-] \qquad \text{Equation 3.5}$$

The second-order rate constant for deuterioxide ion-catalyzed exchange may be obtained as the slope of a plot of k_{obs} values against the concentration of deuterioxide ion.

Finally, the second-order rate constants for deuterioxide ion-catalyzed exchange k_{DO} ($M^{-1}s^{-1}$) can be used to estimate pK_a values for the imidazolium ions studied by providing access to k_{HO} values for hydroxide ion-catalyzed deprotonation (Scheme 3.2, Equation 3.6).[41]

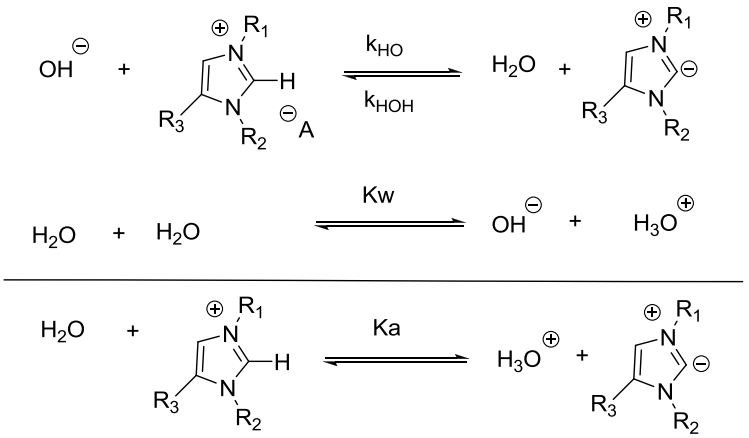

Scheme 3.2 Hydroxide ion-catalyzed deprotonation

$$pK_a = pK_w + \log(\frac{k_{HOH}}{k_{HO}})$$ Equation 3.6

The secondary solvent isotope effect relationship, k_{DO}/k_{HO} =2.4[42], may thus be applied where proton transfer occurs in a pre-equilibrium.

In this way, the values of k_{HO} can be obtained from the experimental k_{DO} values. This secondary solvent isotope effect results from the higher basicity of deuterioxide ion in D_2O, compared to hydroxide ion in H_2O.

The rate constant for the reorganization of solvent k_{reorg} has been estimated to be equal to that for the dielectric relaxation of water, 10^{11} s^{-1}.[43] Thus the rate constant for reprotonation of the carbene or ylide by water, k_{HOH}, may be equated with the rate constant for solvent reorganization according to Equation 3.7.[44, 45]

$$k_{HOH} = k_{reorg} \approx 10^{11} s^{-1}$$ Equation 3.7

As for thermodynamic acidity, it measures compound's pK_a by observing chemical shift on NMR spectra. The background thermochemistry rationale is listed below.[22-24]

For the ionization reaction process of AH in water: $AH + H_2O \rightleftharpoons A + H_3O^+$

K_a can be considered as the ionization constant of this reaction

The observed chemical shift of base A on NMR is populational shift of protonated and deprotonated forms (see Equation 3.8). X_{AH} and X_A represent the population of each form in the whole system.

$$\delta_{obs} = \delta_{AH} X_{AH} + \delta_A X_A \qquad \text{Equation 3.8}$$

Since the sum of X_{AH} and X_A always equals to 1. Equation 3.8 could be transformed into Equation 3.9

$$X_{AH} = \frac{\delta_{obs} - \delta_A}{\delta_{AH} - \delta_A} \qquad \text{Equation 3.9}$$

Besides, K_a and pK_a can be expressed as below (Equation 3.10).

$$K_a = \frac{[H_3O^+][A]}{[AH]} \qquad pK_a = pH + \log\frac{[AH]}{[A]} \qquad \text{Equation 3.10}$$

In equation 3.10, the [AH] and [A] can be replaced by XAH and XA in equation 3.11

$$pK_a = pH + \log\frac{X_{AH}}{X_A} \qquad \text{Equation 3.11}$$

Finally, it seems that the only unknown variables in equation 3.11 are δ_{AH} and δ_A. The way to acquire δ_{AH} and δ_A is through a graph of chemical shift as a function of pH in Figure 3.2.

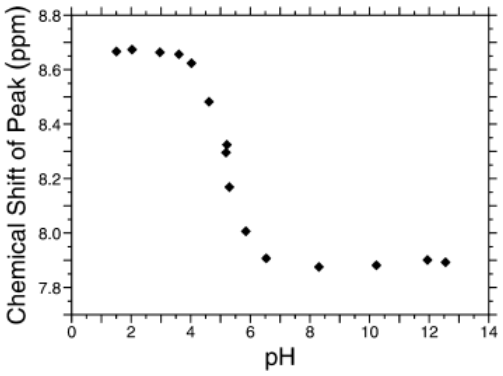

Figure 3.2 chemical shift of a proton on compound as a function of pH

From the graph in figure 3.2, two platforms on each ends of the curve represent the average of chemical shift in a form of protonated compound (δ_{AH}) and a form of deprotonated compound (δ_A).

3.2 Results and discussion

3.2.1 Calculational PA and experimental PA

The structures are optimized at B3LYP/6-31+G(d) level and PA (calc, gas) are calculated on this level. The cpcm calculation is based on the optimized structure at B3LYP/6-31+G(d) scrf=(cpcm, read, solvent=water) and $\Delta\Delta G_{solvation}$ is obtained by cpcm calculation "total free energy in solution: with all non electrostatic terms". The proton affinity (PA) are measured using bracketing method in LCQ.

The Strassner ionic liquids that we have studied in this project and their PA_{gas} calculations are shown in Figure 3.3

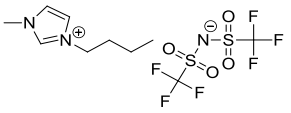

[BMIM][NTf_2]

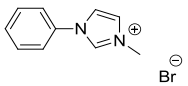

TT116

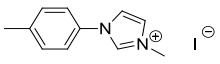

TT1436

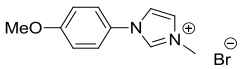

TT29

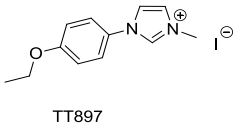

TT897

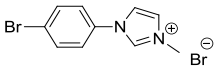

TT26

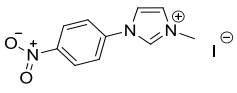

TT1458

Ionic Liquids	PAcal (kcal/mol)	PAexp (kcal/mol)*
TT1458	251.1	252.1±3
TT26	258.4	258.8±3
TT116	261.4	261.3±3

[BMIM][NTf_2]	262.6	262.9±3
TT1436	263.1	262.9±3
TT29	264.2	>263.8
TT897	264.8	>263.8

Figure 3.3 Structures and names of Strassner ionic liquids studied and their calculated PA_{gas} and experimental PA_{gas}*

*TT26,TT116, TT29 were measured by Sisi Zhang[9]. Calculation work is done by using B3LYP/6-31+G(d) method. The experimental PA results are derived from bracketing kinetics method on LCQ.

As we can see from the data above, the results demonstrate the relationship between the para-substituent on aryl group and gas phase acidity. TT1458, TT26 (with electron-withdrawing group) do have low ΔH_{acid}, while TT897, TT29 (with electron -donating group) have higher ΔH_{acid}.

3.2.2 Thermodynamic pK_a measurements

Chemicals hydrogen chloride, potassium hydroxide, tetramethylamine bromide, dueterioxide are commercially available. Solvent are not refluxed before use. ^1H NMR were recorded in D_2O with internal standard tetramethylamine bromide on Varian vnmrs 300 spectrometers as noted. Data for ^1H NMR are reported as follows: chemical shift (δ ppm), multiplicity (s=singlet, d=doublet, t=triplet, q=quartet, qt=quintet, m= multiplet), integration, and assignment.

The deuterated chloride acid and potassium hydroxide were prepared to modulate the pH of the sample dissolved in deuterium oxide containing internal standard tetramethylamine bromide. Then NMR spectra were taken under different pH conditions. (see Figure 3.4)

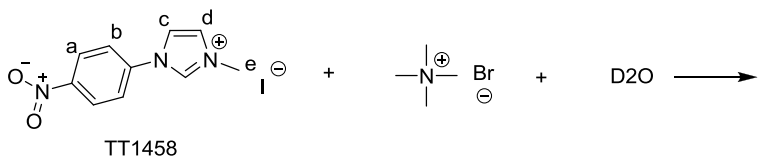

TT1458

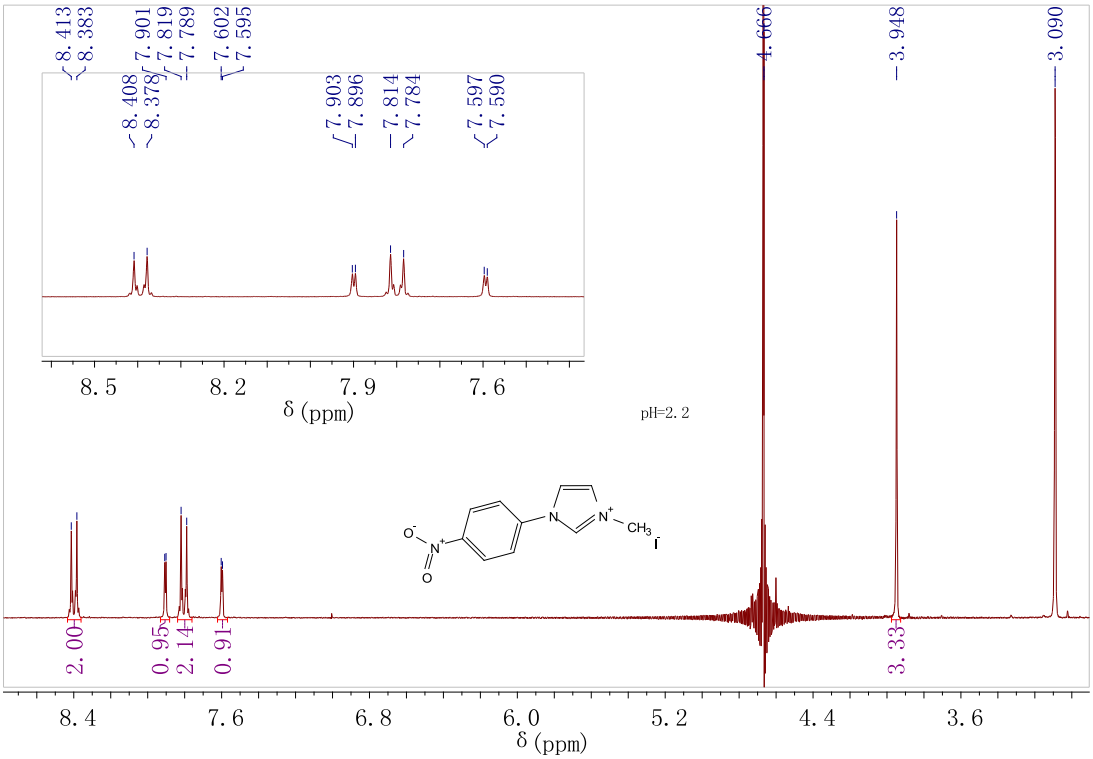

^{1}H NMR of the sample at pH=2.2

^{1}H NMR (300 MHz, D_2O) δ 8.40 (m, 2H, ArH_a), 7.90 (d, 1H, H_d), 7.80 (m, 2H, ArH_b), 7.60 (d, 1H, H_c), 3.95 (s, 3H, $N(CH_3)$), 3.10 (s, $N(CH_3)_4$)

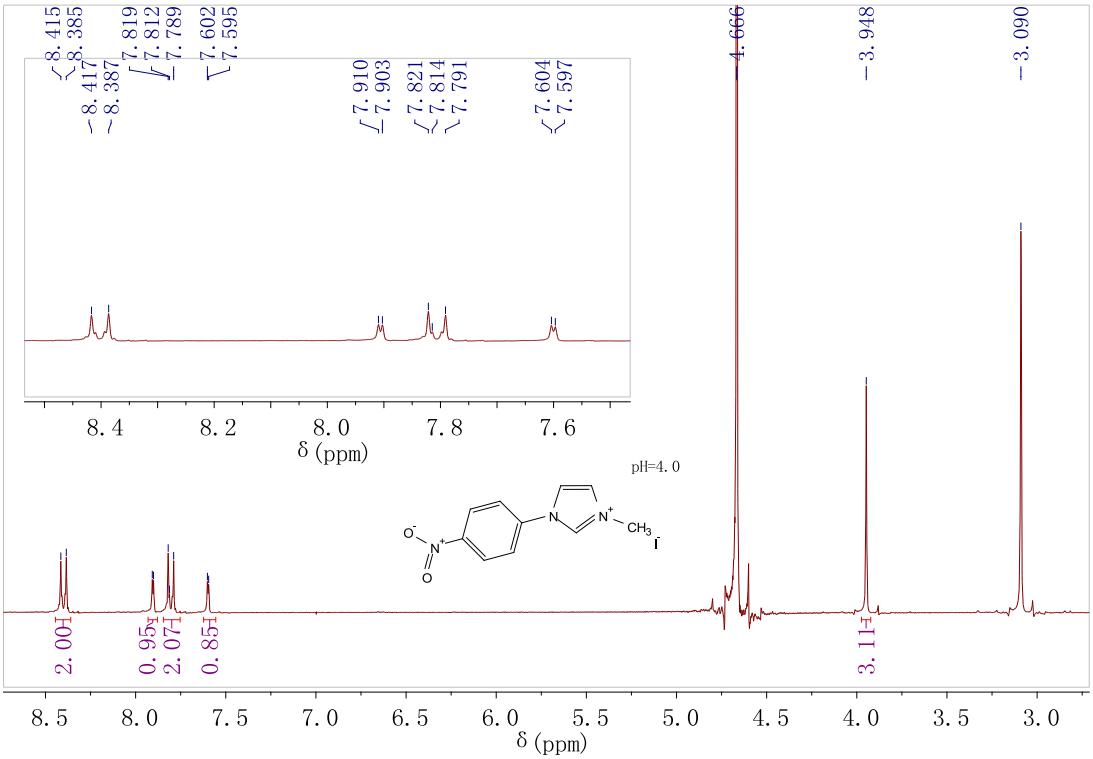

^{1}H NMR of the sample at pH=4.0

^{1}H NMR (300 MHz, D_2O) δ 8.40 (m, 2H, ArH_a), 7.90 (d, 1H, H_d), 7.80 (m, 2H, ArH_b), 7.60 (d, 1H, H_c), 3.95 (s,3H, $N(CH_3)$), 3.10 (s, $N(CH_3)_4$)

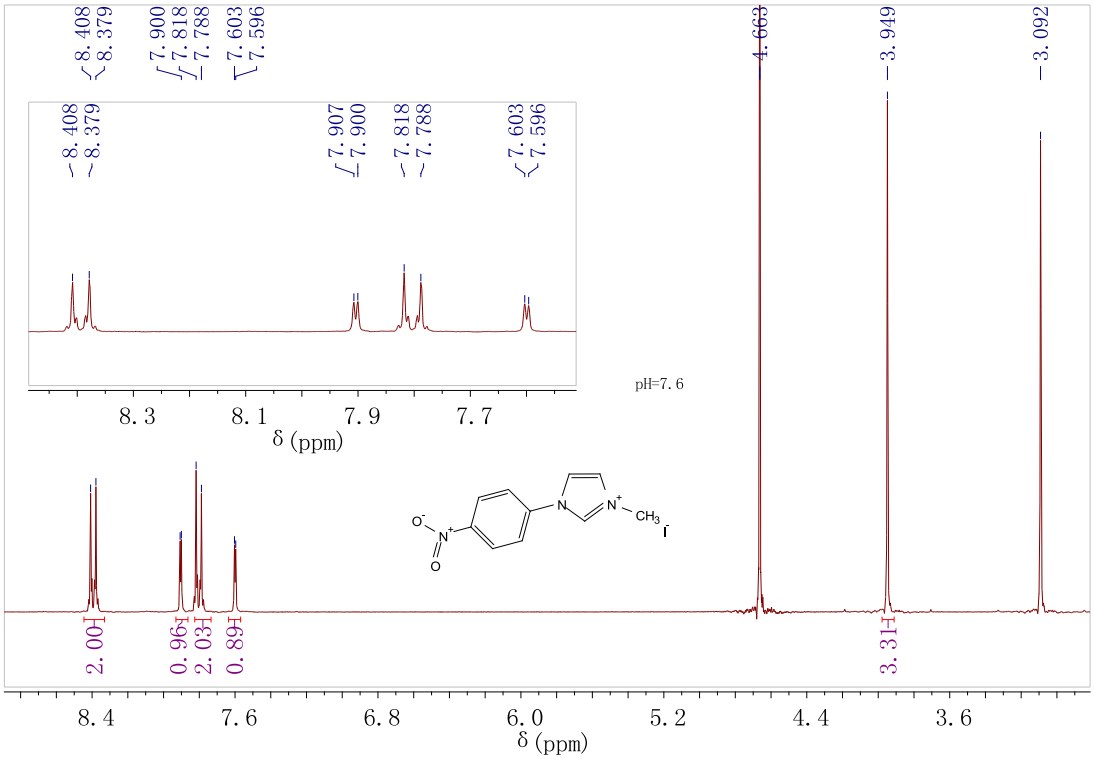

^{1}H NMR of the sample at pH=7.6

^{1}H NMR (300 MHz, D_2O) δ 8.40 (m, 2H, ArH_a), 7.90 (d, 1H, H_d), 7.80 (m, 2H, ArH_b), 7.60 (d, 1H, H_c), 3.95 (s,3H, $N(CH_3)$), 3.10 (s, $N(CH_3)_4$)

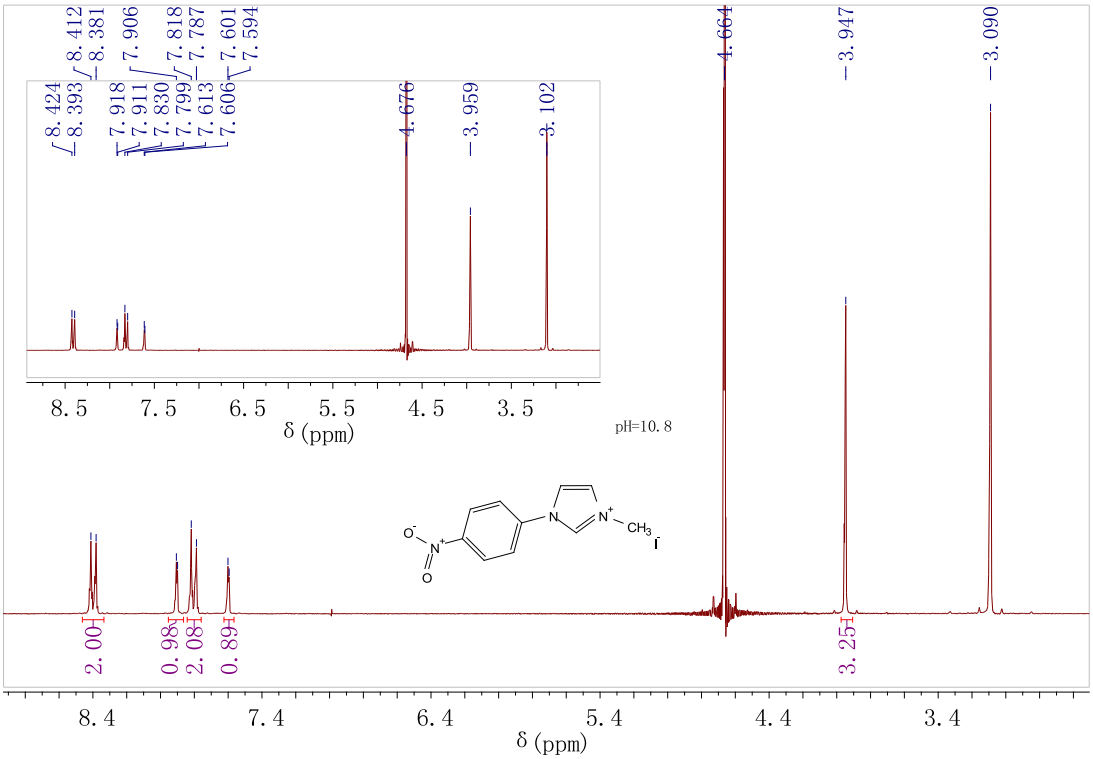

^{1}H NMR of the sample at pH=10.8

^{1}H NMR (300 MHz, D_2O) δ 8.42 (m, 2H, ArH_a), 7.91 (d, 1H, H_d), 7.83 (m, 2H, ArH_b), 7.60 (d, 1H, H_c), 3.95 (s,3H, $N(CH_3)$), 3.10 (s, $N(CH_3)_4$)

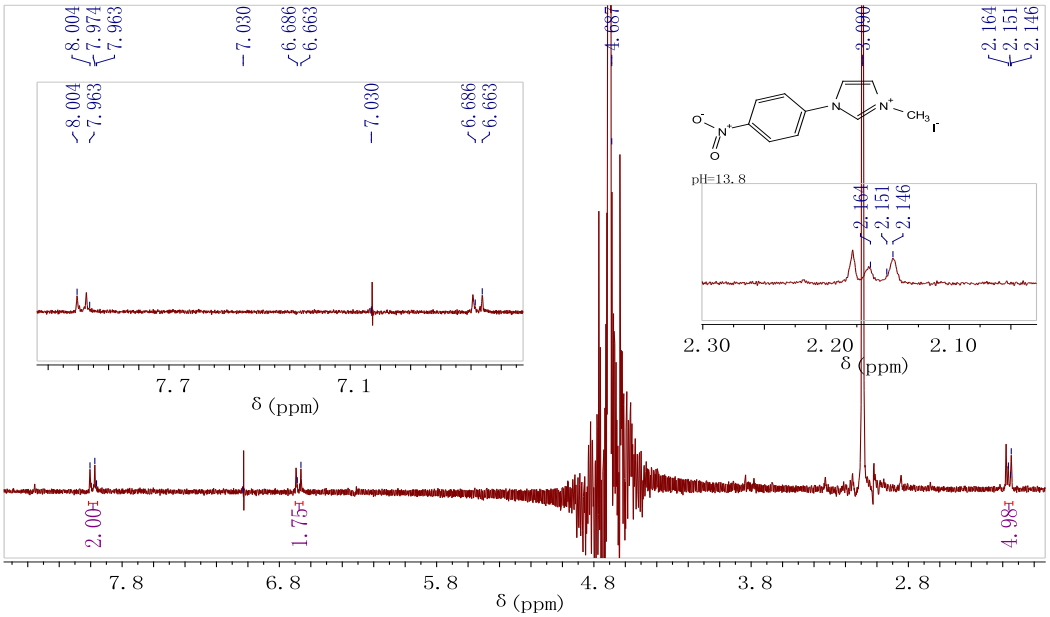

^{1}H NMR of the sample at pH=13.8

^{1}H NMR (300 MHz, D_2O) δ 8.00 (m, 2H, ArH_a), 6.69 (m, 2H, ArH_b), 2.15(M, 5H), 3.10 (s, $N(CH_3)_4$)

Figure 3.4 NMR spectra of ionic liquid TT1458 at five pHs

After collecting all the data, the plot of chemical shift of b protons (Hb) on TT1458 vs pH profile is below (Figure 3.5)

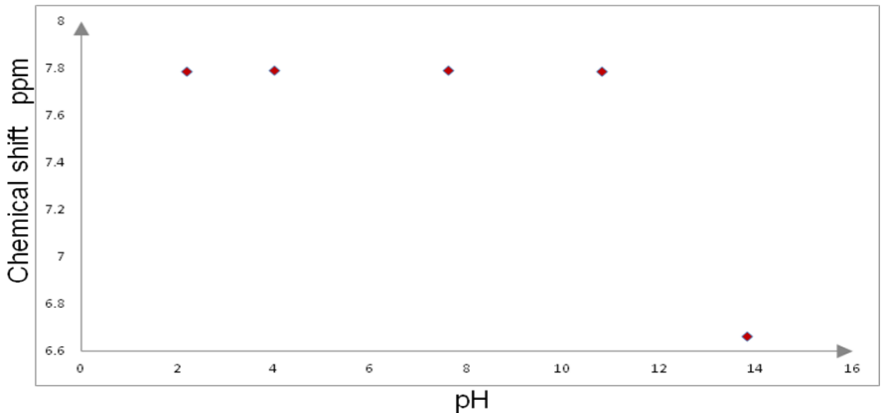

Figure 3.5 Chemical shift of b protons on TT1458 vs pH profile

However, two problems were found lying behind this method. Firstly, this thermodynamic acidity measurement is impracticable for imidazolium-based ionic liquid TT1458 since OH^- is not basic enough to deprotonate the Strassner carbene completely. Based on the curve obtained, it seems that the platform may extend beyond pH~15 which is the pK_a of H_2O. That means the basicity of H_2O limits getting plots to finish the platform part of the curve. Secondly, some yellow precipitate were observed when the solution became more basic. It is very doubtful that whether the ^1H NMR spectra at pH=13.8 reflects deprotonated TT1458. Obviously, the peaks of protons on imidazolium core H_a and H_b are gone, the same with the methyl proton peak. The unknown structure might be some impurity or dimer. In order to comfirm the structure, the solution with precipitate was added with acetonitrile. After the

whole system become homogeneous, 20 uL sample at the concentration of 1-10mg/ml was taken inside LC-UV-MS to test m/z of the species it may involve. m/z (TT1458 cation)=204.08

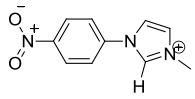

m/z=204.08

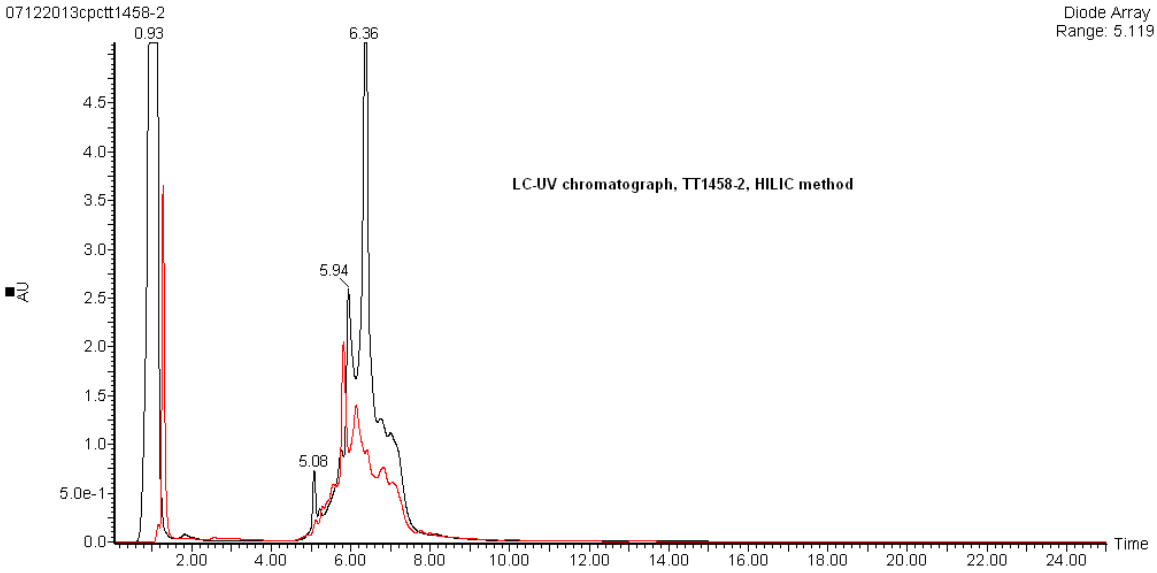

Figure 3.6 LC-UV chromatograph, 254-255.5nm for TT1458 for two times

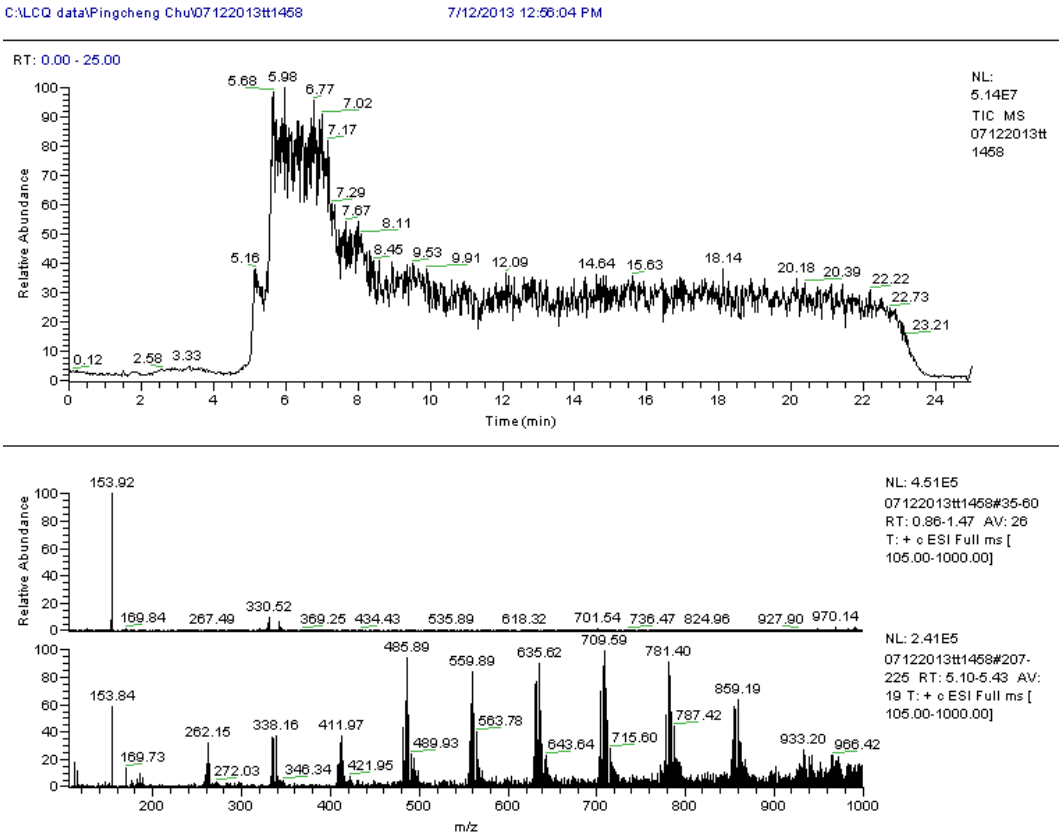

Figure 3.7 LC-MS chromatograph fullscan of TT1458 for 0-25mins, 0.86-1.47mins, 5.10-5.43mins

07122013tt1458_130712144945 7/12/2013 2:49:45 PM

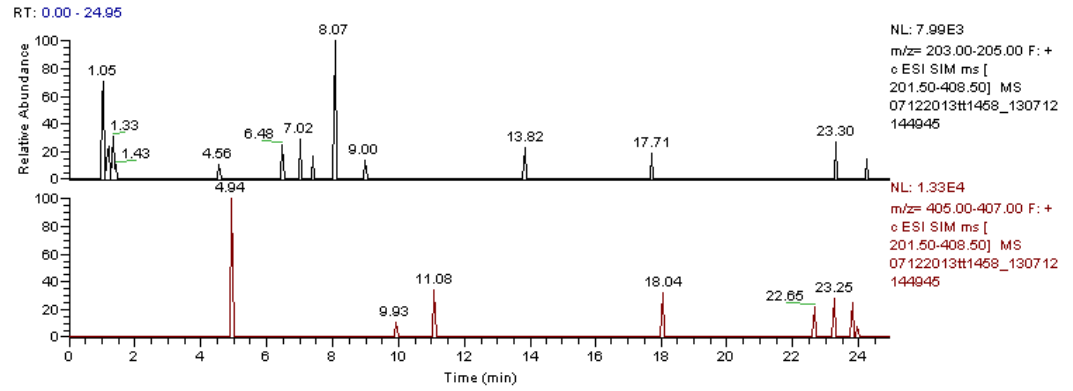

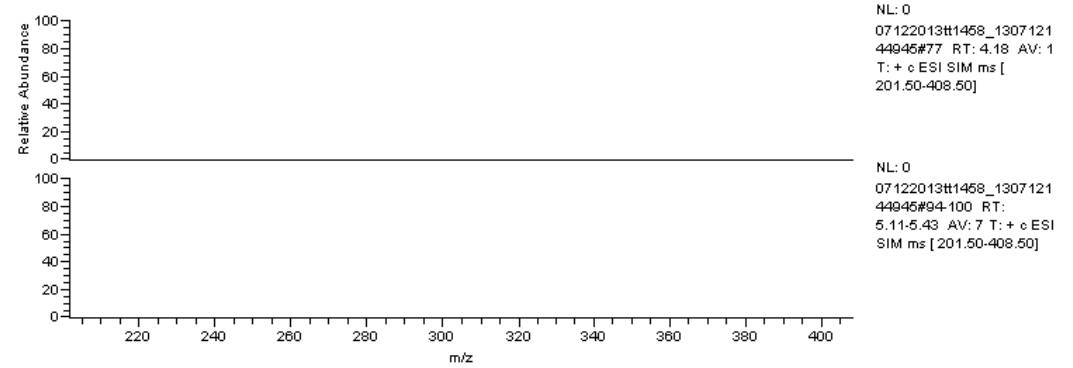

07122013tt1458_130712144945 7/12/2013 2:49:45 PM

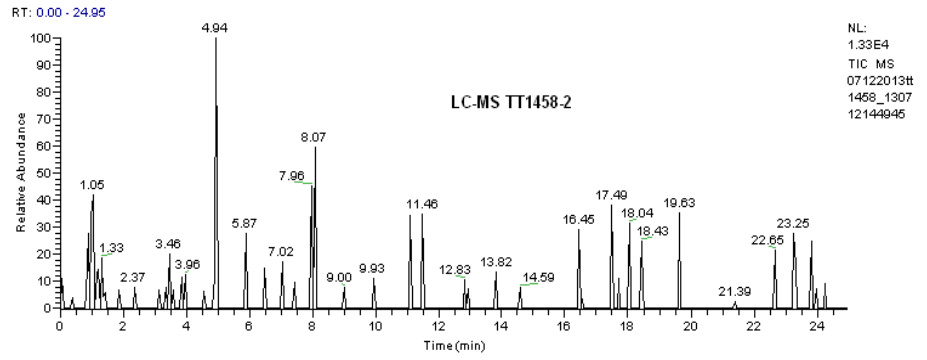

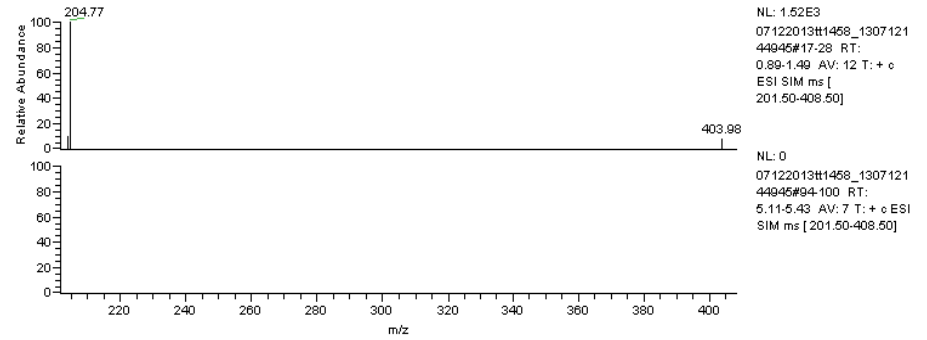

Figure 3.8 LC-MS chromatograph SIM of TT1458 at m/z=203-205, 405-407

(first trial, above. Second trial, bottom)

Figure 3.6 is LC-UV chromatograph, 254-255.5nm for TT1458. The experiments were done twice. As for the second trial, we increase the injection volum from 10 uL to 25 uL to get best signal. The peaks in chromatograph show that some components in TT1458 solution absorb UV wavelength from 254-255.5 nm at retention time around 5-7 mins. The large peak at retention time around 1 min might be void which is further verified by that no peak but m/z=154 appearing in the LC-MS spectra of retention time between 0.86-1.47 mins. The peak of m/z=154 might be one reference base MTBD which is left inside ion trap from previous tests. Similarly, when we looked into SIM spectra of 203-205 and SIM spectra of 405-407, no significant peaks of m/z=204 or 407 could be observed. Also, the poor response to the baseline in TIC might be resulted to the bad sensitivity of the machine or the non-existence of components corresponding to the targeted m/z. Thus, we are unable to conclude anything from the LC-MS results. In sum, measuring pK_a by thermodynamic acidity method does not work. In order to solve the problem, we turned to use kinetics method via H/D exchange reaction on NMR.

3.2.3 pK_a measurement by kinetics acidity

Chemicals including potassium phosphate monobasic, potassium phosphate

dibasic, ionic strength control solution KCl (I=1.0) were used as provided from commercial purchase. Deuterated potassium phosphate monobasic and deuterated potassium phosphate dibasic were prepared according to reported procedures[46].

^{1}H NMR were recorded in D_2O with internal standard tetramethylamine bromide on Varian vnmrs 500 spectrometers as noted. Data for ^{1}H NMR are reported as follow chemical shift (δ ppm), multiplicity (s=singlet, d=doublet, t=triplet, q=quartet, qt=quintet, m=multiplet), integration, and assignment.

3.2.3.1 Preparation of buffer solutions

Stock solutions of buffers, K_2DPO_4 and KD_2PO_4 were obtained from potassium phosphate monobasic (KH_2PO_4) and dibasic (K_2HPO_4) by exchanging the hydrogen atoms for deuterium. 2.05g K_2HPO_4 (M.W=174.18 g/mol) and 2.5g KH_2PO_4 (M.W=136.09 g/mol) were taken to be dissolved in 5-8 mL D_2O, followed by removal of solvent by evaporation under reduced pressure at Dr. Seidel's lab. The process was repeated five times and the salts were freeze dried at Dr. Roger Jones' lab. The amount of K_2DPO_4 is 1.97g and KD_2PO_4 is 2.214g. They were kept in the desiccator. Then NMR spectra of them indicate the full degree of deuteration due to no signal for protons. 0.175g K_2DPO_4 and 0.138g KD_2PO_4 were taken to prepare 10 mL 0.1 mol/L stock solution. The phosphate buffers with different pD were prepared by mixing stock solutions of K_2DPO_4 and KD_2PO_4 in D_2O with addition of KCl to

give solutions of buffer at various acid/ base ratios in Table 3.1 and I = 1.0 (KCl).

pD	components	quantity
6.52	K_2DPO_4 27.8%	3.475 mL
	KD_2PO_4 72.2%	9.025 mL
	KCl	0.9320 g
6.72	K_2DPO_4 38.1%	1.905 mL
	KD_2PO_4 61.9%	3.095 mL
	KCl	0.3738 g
6.93	K_2DPO_4 50%	2.0 mL
	KD_2PO_4 50%	2.0 mL
	KCl	0.298 g
7.17	K_2DPO_4 60%	2.4 mL
	KD_2PO_4 40%	1.6 mL
	KCl	0.298 g
7.37	K_2DPO_4 72%	2.88 mL
	KD_2PO_4 28%	1.12 mL
	KCl	0.298 g
7.52	K_2DPO_4 80%	1.6 mL
	KD_2PO_4 20%	0.4 mL
	KCl	0.199 g

Stable 3.1 buffer solutions of K_2DPO_4 and KD_2PO_4 in D_2O with addition of KCl (I=1.0) at different pD

3.2.3.2 Determination of apparent acitivity coefficient

The pD of buffered solutions is determined at 25 ℃ using a Accumet 950 pH/ion Controller equipped with a radiometer (pH 4 - 7 - 10 @ 25 ℃) combination electrode, that could be standardized between pH 4 - 7 or pH 7 - 10 to encompass the pD of the buffer solution. The pD is calculated by adding 0.4 to the observed reading of the pH meter.

The activity coefficient for hydroxide ion was determined from the fit of the observed pH of a series of solutions of known hydroxide concentration at constant ionic strength to Equation 3.12

$$10^{(pH-pKw)} = \gamma_{OH}\,[HO^-] \qquad \text{Equation 3.12}$$

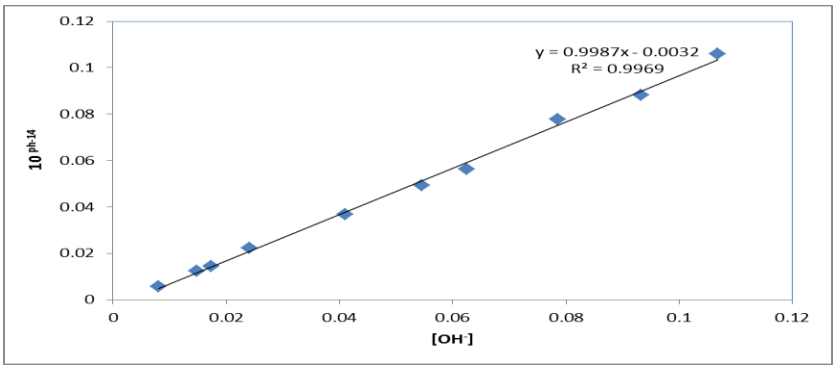

Figure 3.9 Determination of the activity coefficient for hydroxide ion

3.2.3.3 Calculation of [DO^-]

The deuterioxide concentrations were calculated from the equation 3.3 [DO^-] = $(10^{pD - pKw})/ \gamma_{DO}$, where $K_w = 10^{-14.87}$ M^2 is the ion product of D_2O at 25 °C and γ_{DO} = 0.9987 is the apparent activity coefficient of deuterioxide ion under our experimental conditions.

3.2.3.4 ^1H NMR exchange reactions

H/D exchange reactions of imidazolium-based ionic liquid TT1458 were carried out in NMR tubes which were incubated at 25±0.1 ℃ in a thermostated water bath. All reactions were carried out in D_2O with the ionic strength maintained at I = 1.0. 800 uL NMR sample were initiated by injection of buffer and internal standard tetramethylamine bromide to solid substrate. In general, the final substrate and internal standard concentrations in the reaction solutions are 8 mM and 0.8 mM, respectively. For instance, 0.002648 g TT1458 and 0.0001 g tetramethylamine bromide were taken to prepare 800 uL NMR sample.

As for the NMR parameter setting, the relaxation delay between pulses is set to 1 s on 500 MHz NMR. Spectra are recorded at a pulse angle of 45 °, a sweep width of 7022.5 Hz, an acquisition time of 2.049 sec, and 16 transients, pulse width of 45 °and spin of 20 Hz. The kinetics experiment was executed by setting array size of

12 with first value of 0 and last value of 300. Baselines are subject to first–order drift correction before integration of the peak areas.

3.2.3.5 Results and discussion

The NMR spectra of TT1458 H/D exchange at various pD are shown in the Figure 3.7

.

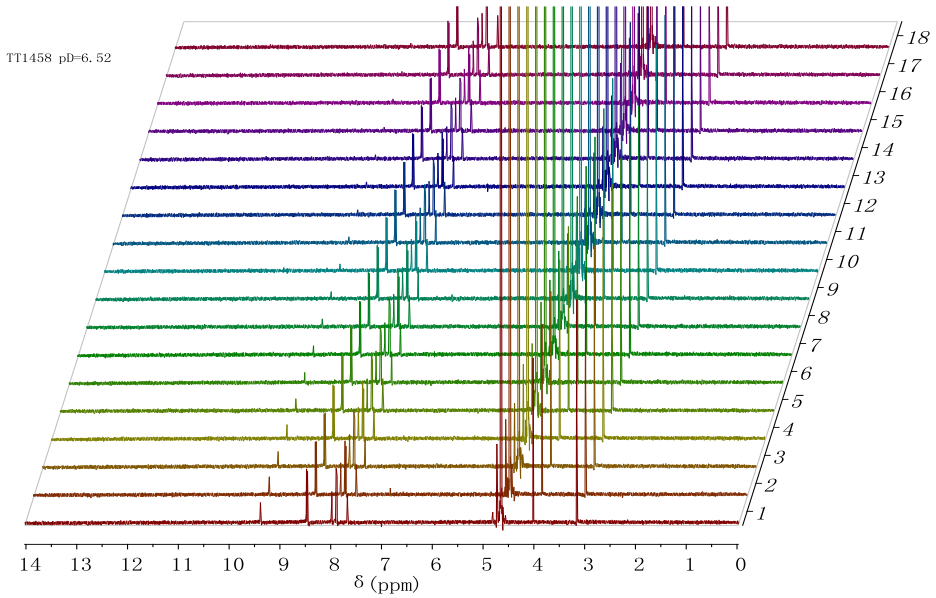

The H/D exchange spectra of TT1458 at pD=6.52

^{1}H NMR (500 MHz, D2O) δ 9.38 (s, 1H, NCHN), 8.42 (m, 2H, ArH_a), 7.91 (d, 1H, H_d), 7.83 (m, 2H, ArH_b), 7.60 (d, 1H, H_c), 3.95 (s,3H, $N(CH_3)$), 3.15 (s, $N(CH_3)_4$)

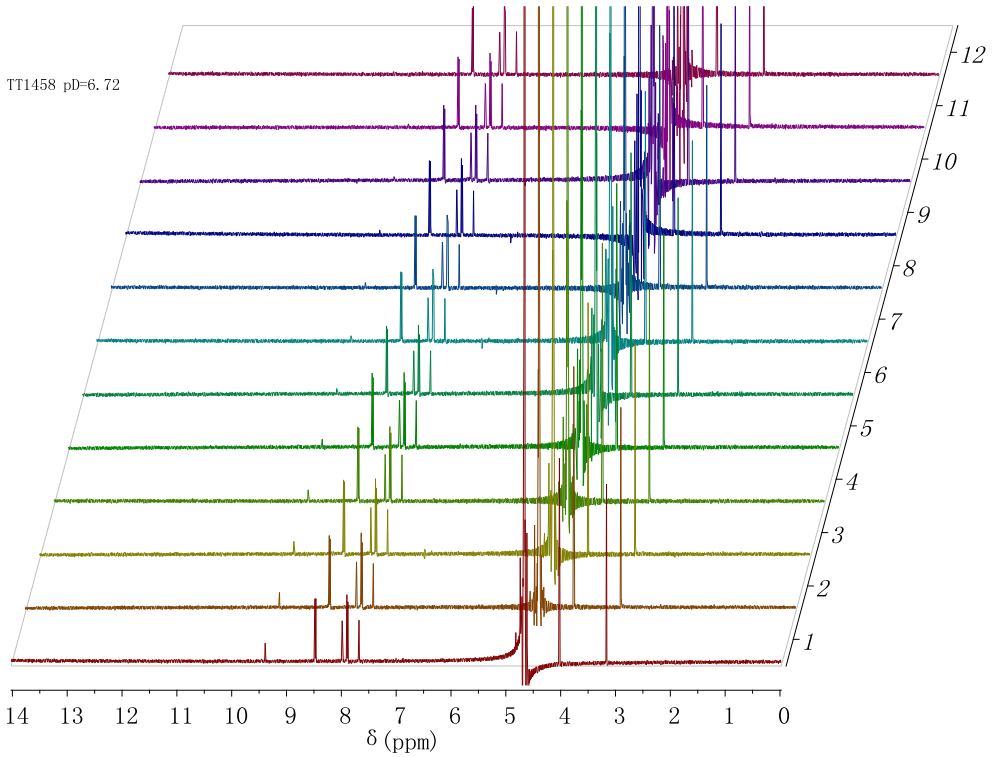

The H/D exchange spectra of TT1458 pD=6.72

^{1}H NMR (500 MHz, D_2O) δ 9.38 (s, 1H, NCHN), 8.42 (m, 2H, ArH_a), 7.91 (d, 1H, H_d), 7.83 (m, 2H, ArH_b), 7.60 (d, 1H, H_c), 3.95 (s,3H, $N(CH_3)$), 3.15 (s, $N(CH_3)_4$)

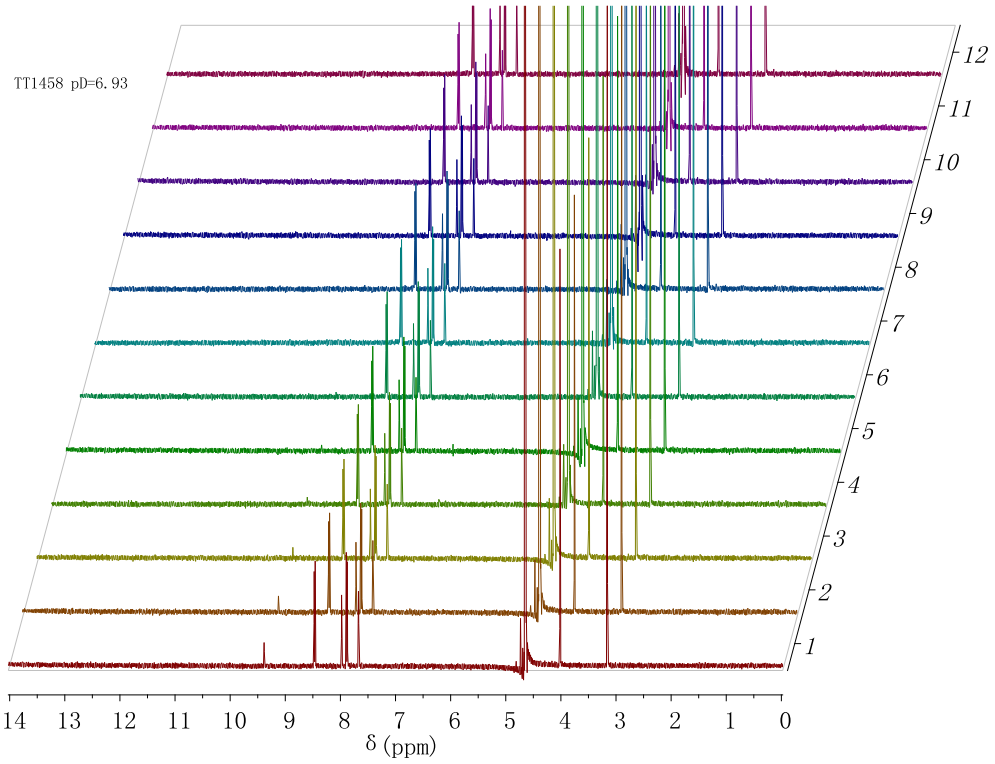

The H/D exchange spectra of TT1458 pD=6.93

^{1}H NMR (500 MHz, D_2O) δ 9.38 (s, 1H, NCHN), 8.42 (m, 2H, ArH_a), 7.91 (d, 1H, H_d), 7.83 (m, 2H, ArH_b), 7.60 (d, 1H, H_c), 3.95 (s,3H, $N(CH_3)$), 3.15 (s, $N(CH_3)_4$)

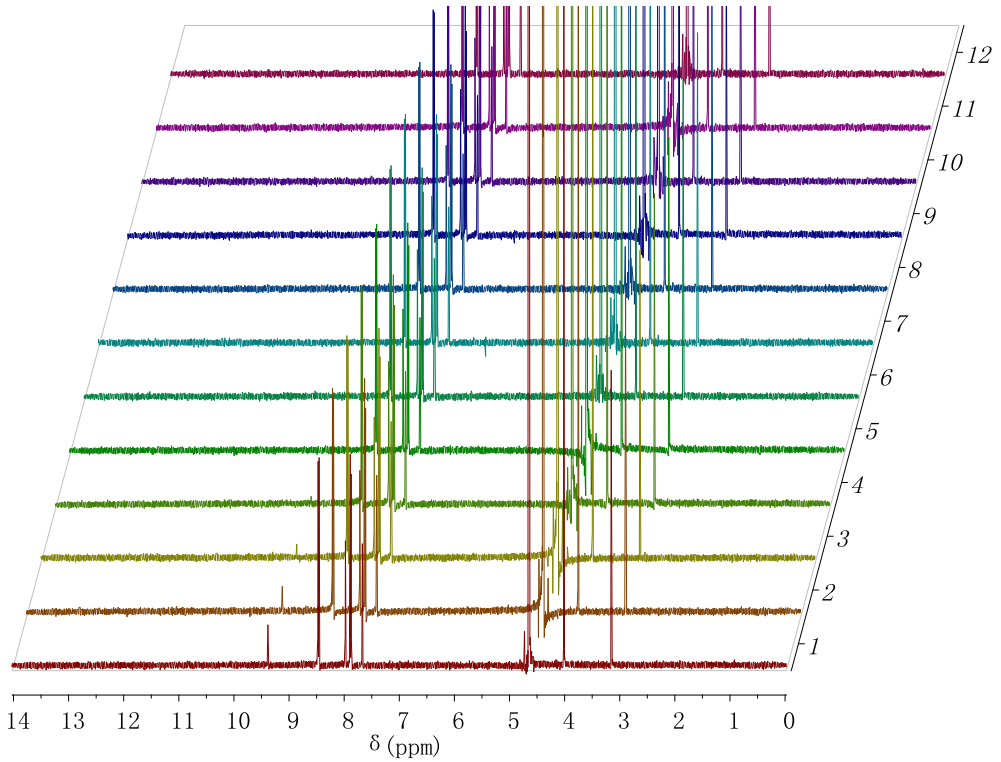

The H/D exchange spectra of TT1458 pD=7.17

^{1}H NMR (500 MHz, D_2O) δ 9.38 (s, 1H, NCHN), 8.42 (m, 2H, ArH_a), 7.91 (d, 1H, H_d), 7.83 (m, 2H, ArH_b), 7.60 (d, 1H, H_c), 3.95 (s,3H, $N(CH_3)$), 3.15 (s, $N(CH_3)_4$)

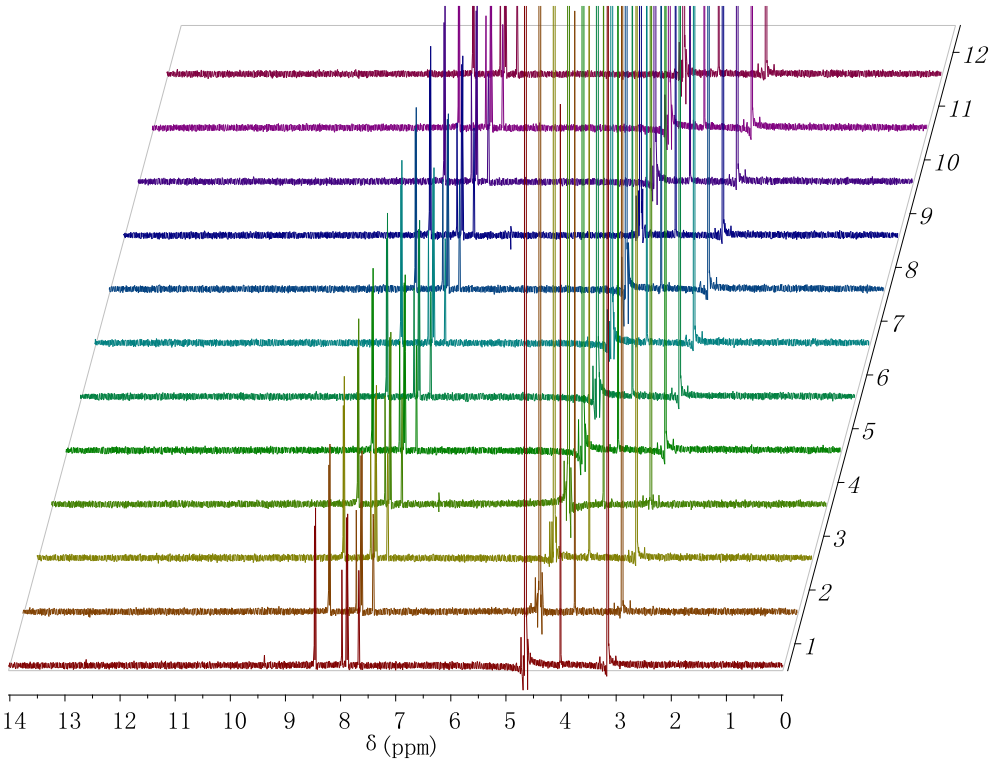

The H/D exchange spectra of TT1458 pD=7.37

^{1}H NMR (500 MHz, D_2O) δ 9.38 (s, 1H, NCHN), 8.42 (m, 2H, ArH_a), 7.91 (d, 1H, H_d), 7.83 (m, 2H, ArH_b), 7.60 (d, 1H, H_c), 3.95 (s,3H, $N(CH_3)$), 3.15 (s, $N(CH_3)_4$)

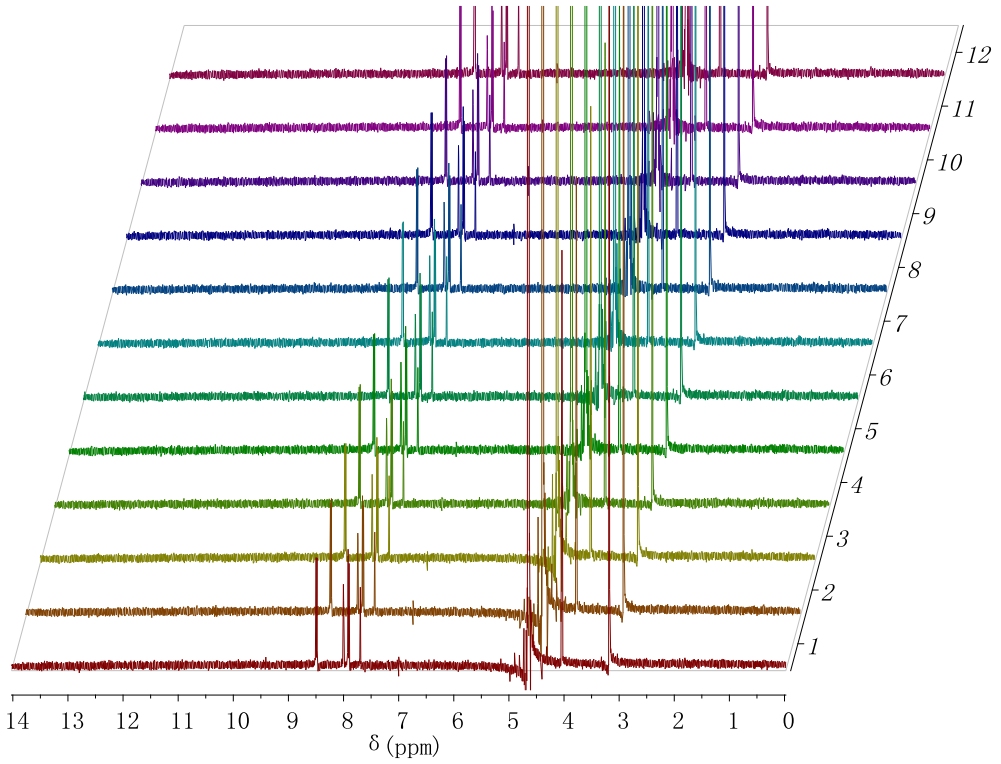

The H/D exchange spectra of TT1458 pD=7.52

^{1}H NMR (500 MHz, D_2O) δ 8.42 (m, 2H, ArH_a), 7.91 (d, 1H, H_d), 7.83 (m, 2H, ArH_b), 7.60 (d, 1H, H_c), 3.95 (s,3H, $N(CH_3)$), 3.15 (s, $N(CH_3)_4$)

Figure 3.10 NMR spectra of H/D exchange reaction of TT1458 at various pD

From those spectra shown above, the chemical shift of peak for C2-H imidazolium is around 9.38 ppm and the chemical shift of peak for protons on internal standard is around 3.15 ppm. The integration of those two peaks were obtained after first-order baseline correction. Then plug those integration into equation 3.1 to obtain f(s), followed with calculating the k_{obs} via equation 3.2, finally estimating second-order rate constant k_{OD} via equation 3.5. The concentration of DO^- is calculated by equation 3.3. Figure 3.11 gives out k_{obs} (s^{-1}) values as the slopes of those plots between lnf(s) and time for deuterioxide ion-catalyzed H/D exchange of the

C2-H of TT1458. All the corresponding integration, f(s), lnf(s) and four k_{obs} values are listed as below in Table 3.2.

pD [DO^-]	Time (s)	Integration		f(s)	lnf(s)	k_{obs} (s-1)
		A_{C2-H}	A_{Std}			
6.52	48.784	1	5.77	1	0	
4.47265E-09	397.568	1	6.88	0.838663881	-0.17595	
	746.352	1	6.96	0.829024066	-0.18751	0.0004
	1095.136	1	8.16	0.707108762	-0.34657	
	1443.92	1	9.34	0.617773822	-0.48169	
	1792.704	1	11.48	0.502613894	-0.68793	
	2141.488	1	12.59	0.458300834	-0.78023	
	2490.272	1	15.13	0.381362029	-0.96401	
6.72	48.784	1	5.66	1	0	
7.08867E-09	397.568	1	7.2	0.786113092	-0.24065	
	746.352	1	9.11	0.621296846	-0.47595	0.0008
	1095.136	1	11.6	0.487932264	-0.71758	
	1443.92	1	15.43	0.366818812	-1.00289	
	1792.704	1	22.1	0.256109243	-1.36215	
	2141.488	1	27.01	0.209552546	-1.56278	

6.93	48.784	1	14.48	1	0	
1.14965E-08	397.568	1	22.35	0.647882	-0.43405	
	746.352	1	35.21	0.411251	-0.88855	0.0013
	1095.136	1	55.58	0.260528	-1.34504	
	1443.92	1	73.4	0.197277	-1.62315	
	1792.704	1	157.13	0.092154	-2.38429	
7.17	48.784	1	3.7	1	0	
1.99786E-08	397.568	1	6.61	0.559758	-0.58025	
	746.352	1	12.42	0.297907	-1.21097	0.0018
	1095.136	1	25.09	0.147469	-1.91414	
7.37	48.784	1	92.39			
	397.568	1	269.26			

Table 3.2 First-order rate constants for exchange of the C2-H of TT1458 for deuterium in phosphate buffers in D_2O at 25℃ and I=1.0 (KCl)

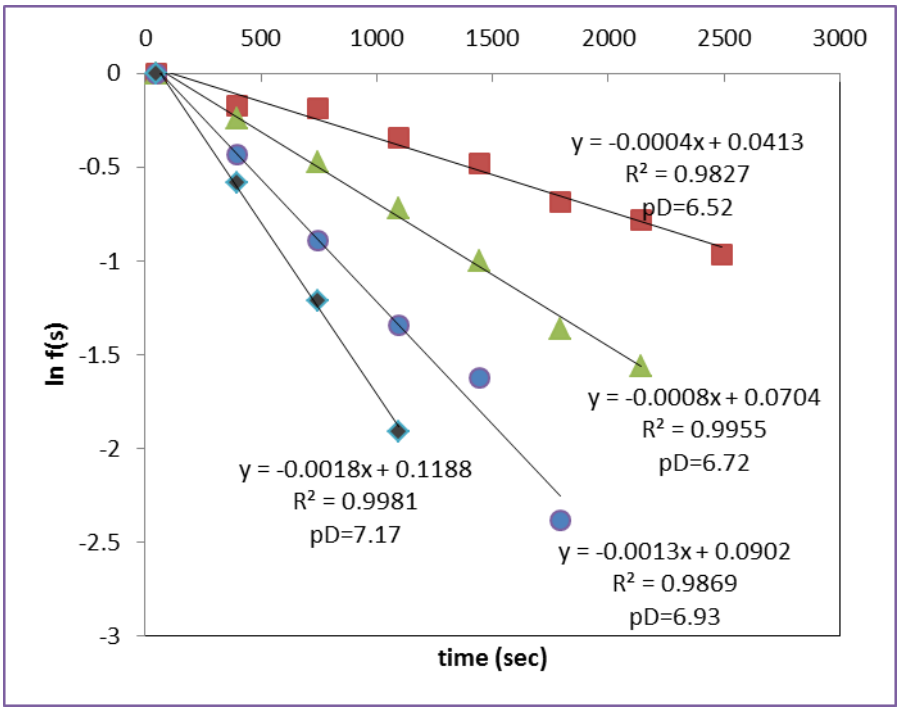

Figure 3.11 Semi-logarithmic plot of the fraction of remaining C2-H against time for the exchange reaction of TT1458 in phosphate buffers in D_2O at 25 ℃ and I=1.0 (KCl): ■ , 27.8% f_B, pD 6.52; ▲, 38.1% f_B, pD 6.72; ● , 50% f_B, pD 6.93; ◆,60% f_B, pD 7.17.

After obtaining k_{obs} at different pD, the second-order rate constants, k_{OD} ($M^{-1}s^{-1}$) value could be acquired as the slope of the plot for deuterioxide ion-catalyzed H/D exchange of the C2-H of TT1458 in figure 3.12. In our experiment, k_{OD} is 0.8735 $M^{-1}s^{-1}$.

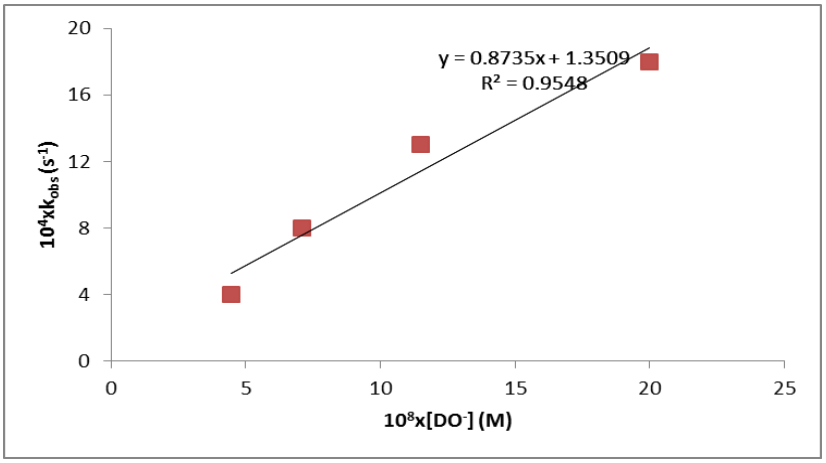

Figure 3.12 Deuterioxide-rate profile for the deuterium exchange reactions of TT1458 in D_2O at 25 ℃ and I=1.0 (KCl)

After k_{DO} is known, k_{HO} can be obtained by the secondary solvent isotope effect relationship, k_{DO}/k_{HO} =2.4. Since K_{HOH} can be considered equal with dielectric relaxation of water which is 10^{11} S^{-1} in equation 3.7, we can plug k_{HO} and k_{HOH} into equation 3.6, getting the pK_a of TT1458 as 25.4.

3.3 Correlation between pK_a and PA_{gas}

According to Ogretir's publication on quantum chemical studies on acidity-basicity behaviors of some substituted pyridine derivatives [47], the theoretical value of pK_a can be estimated from the thermodynamic cycle with equation 3.13. The Scheme 2.5 gives the detailed explanation of the interrelationship between the gas phases and solution phases.[32]

$$pK_a = \frac{\Delta G_a}{2.303RT}$$
$$= \frac{[\Delta G_g + \Delta G_s(B) - \Delta G_s(BH) + \Delta G_s(H^+)]}{2.303RT}$$

Equation 3.13

$$\Delta G_a = \Delta G_g + \Delta G_s(B) - \Delta G_s(BH) + \Delta G_s(H^+)$$

Equation 3.14

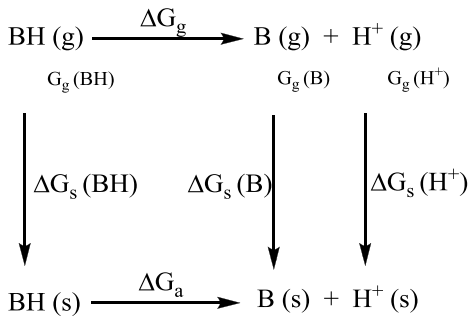

Scheme 3.3 Interrelationship between the gas phase and solution

ΔG_g is the gas phase free energies of ionization
ΔG_a is the solvation free energies of the ionization
ΔG_s's are the solvation free energies of different species
$G_s (H^+)$ = -259.5 kcal/mol [32]

All imidazolium compounds with known experimental pK_a's reported so far have been collected from different publications in Figure 3.13. We may first use them as subjects to investigate the relationship between pK_a and PA_{gas}. All geometry would be optimized by B3LYP/ 6-31+G(d) level and G_g values (for BH, B and H+) as well as PA (calc, gas) would be calculated at this level as well. Afterwards, the single point CPCM calculation would be based on the optimized structure by B3LYP/6-31+G(d) by using scrf=(cpcm, read, solvent=water) and ΔGs values would be obtained by subtracting G_g values from ΔG_{sol} values ("total free energy in solution: with all non electrostatic terms" from CPCM calculation). ΔG_a values would be obtained from equation 3.14. Eventually, pK_a(calc) could be obtained by $(\Delta G_a)/1.36$.

All the thermodynamic properties of imidazolium compounds with known experimental pK_a's are listed in Table 3.3

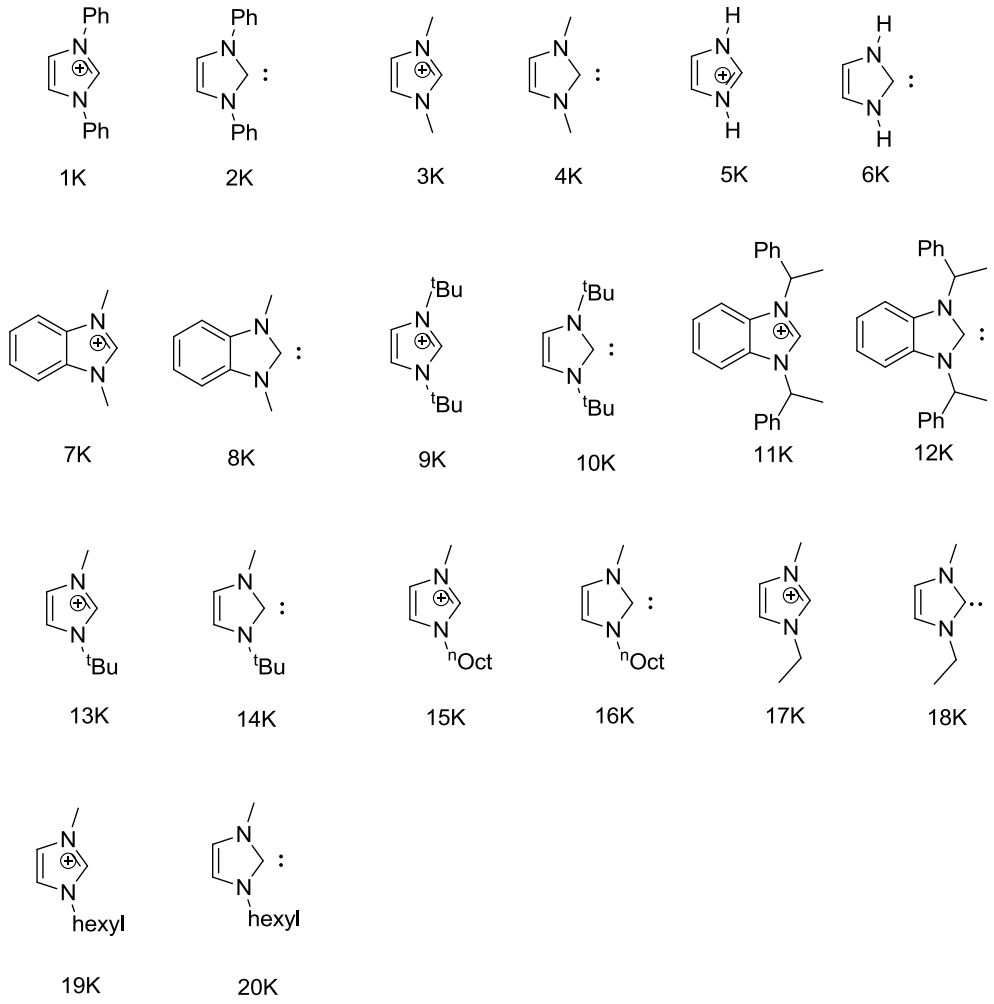

Figure 3.13 All imidazolium compounds with known experimental pK_a's reported so far

Imidazolium compound	Free energy in water Kcal/mol	ΔG_a	$pK_a=\Delta G_a/1.36$	pK_a(exp)
1K	-432220.4462	37.97664114	27.92400084	20
2K	-431916.6896			
3K	-191588.442	45.76654407	33.65187064	23

4K	-191276.8955			
5K	-142257.4535	45.87886827	33.73446196	23.8
6K	-141945.7946			
7K	-288006.447	42.62146646	31.33931357	21.6
8K	-287698.0455			
9K	-338714.8189	34.862939	25.63451397	22.7
10K	-338414.1759			
11K	-627326.1461	43.64932702	32.09509339	21.2
12K	-627016.7168			
13K	-264700.5578	32.45079248	23.86087682	23.3
14K	-264402.327			
15K	-363379.9621	32.23681174	23.70353804	23.4
16K	-363081.9452			
17K	-215359.3302	32.1483329	23.63848007	22.1
18K	-215061.4018			
19K	-314039.6349	32.26316714	23.72291701	23.4
20K	-313741.5918			

Table 3.3 free energy in water, ΔG_a, pK_a(calc), pK_a(exp) of imidazolium compounds 1K-20K

Then we plot pK_a(exp) vs pK_a(calc) by linear fitting in figure 3.14. However, five dots represented by imidazolium compounds 9K, 13K, 15K, 17K, 19K outlie the main trend, which produces a huge derivation. The reason might be from the free energy in water of those four compounds.

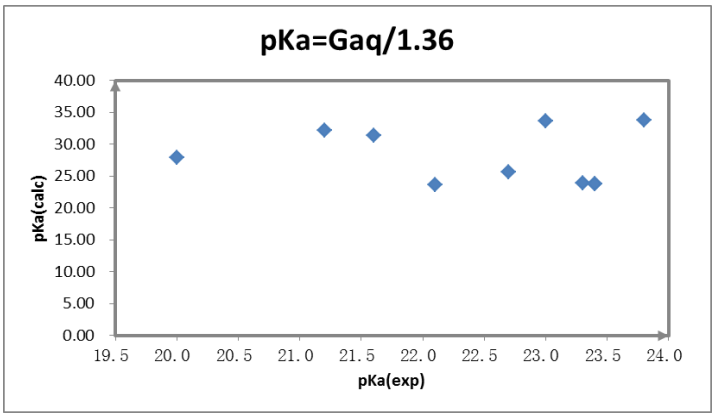

Figure 3.14 plot of pK_a(exp) vs pK_a(calc)

At the same time, we also calculate the ΔG_{sol} of some Strassner compounds in water by CPCM. (Figure 3.15)

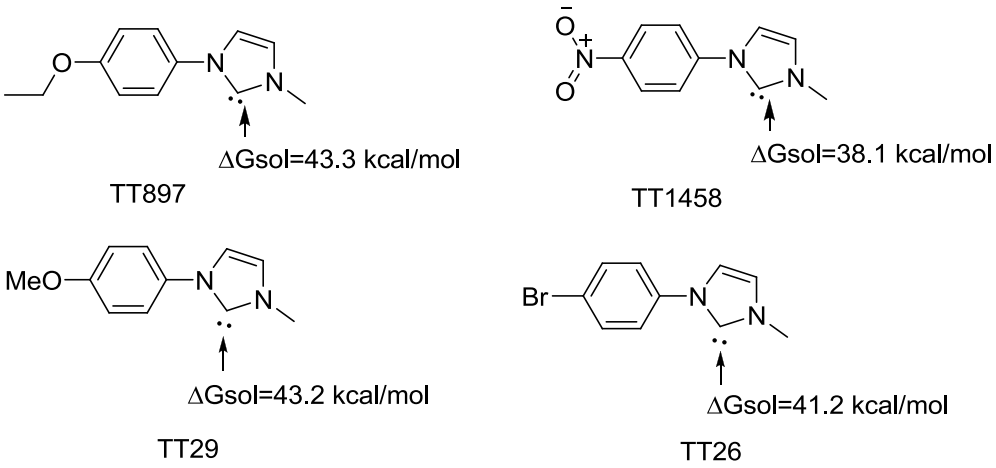

Figure 3.15 ΔG_{sol} in water of Strassner compounds by CPCM, 298K, kcal/mol

3.4 Purification of [BMIM][NTf_2]

Before going on measuring other Strassner compounds, it is necessary to comfirm the purity of those compounds. Herein, one of Strassner

compounds——[BMIM][NTf_2] were characterized by NMR firstly (Figure 3.16). However, we found besides all the assigned peaks for protons on BMIM, there are some other small peaks which could not be recognized. Thus, LC-MS experiment was carried out to test the purity of [BMIM][NTf_2]*.

*with help of group member Landon Greene

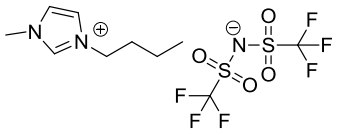

[BMIM][NTf2]

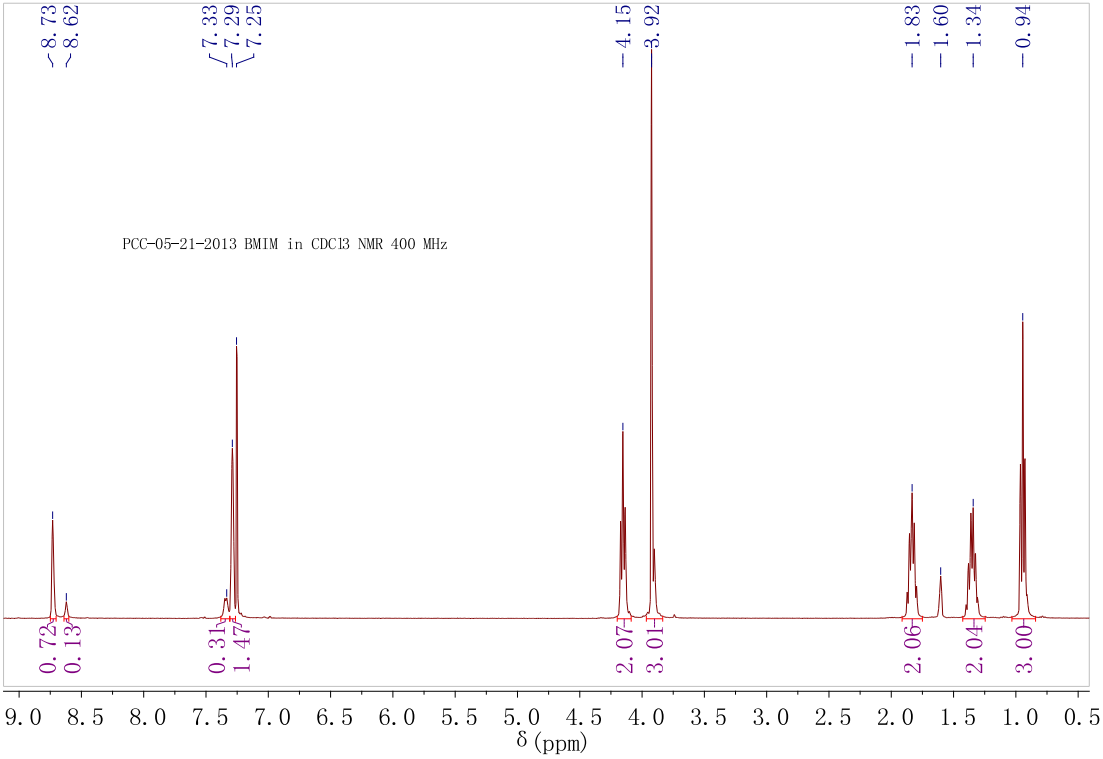

Figure 3.16 NMR spectra of [BMIM][NTf_2]

^{1}H NMR (400 MHz, $CDCl_3$) δ 8.73 (s, 1H, NCHN), 7.29 (m, 2H, NCHC), 4.15 (t, 2H, NCH_2C), 3.92(s, 3H,NCH_3), 1.83(d, 2H, CCH_2C), 1.34 (m,2H,CCH_2C), 0.94(m,3H, CCH_3)

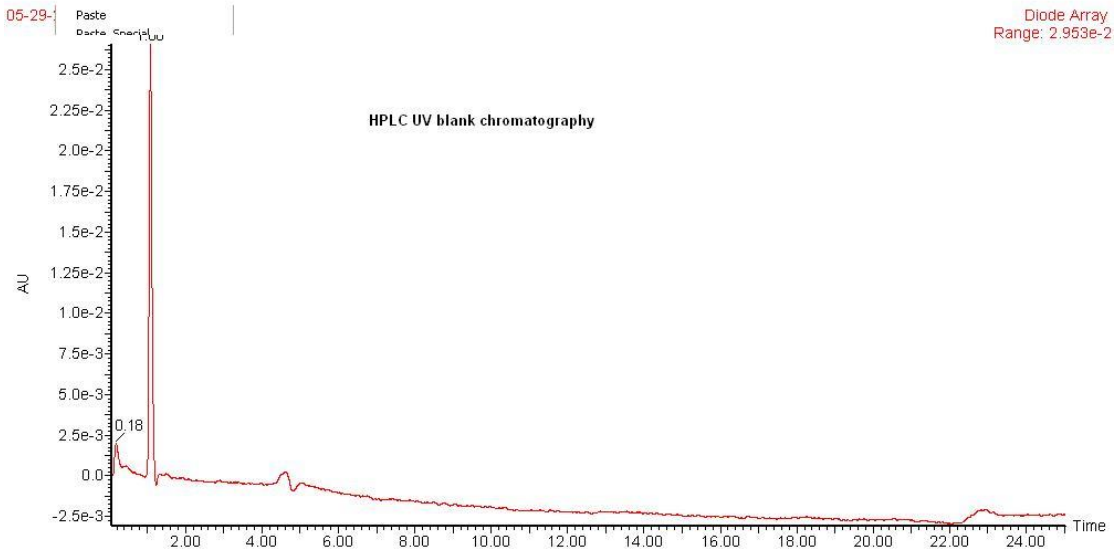

Figure 3.17 LC-UV chromatography of blank

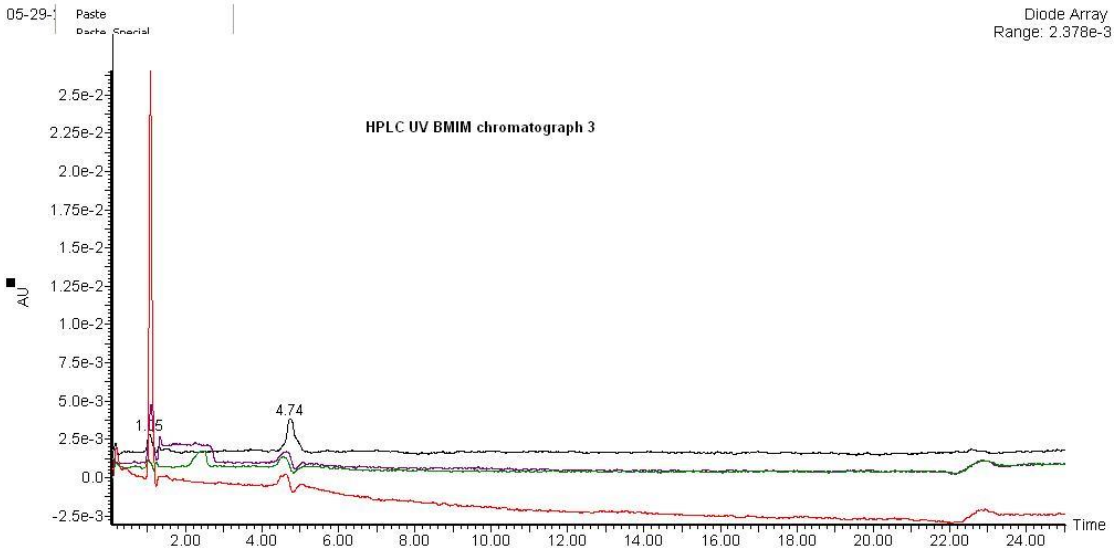

Figure 3.18 LC-UV chromatograph for blank and sample tests of [BMIM][NTf_2] for three times

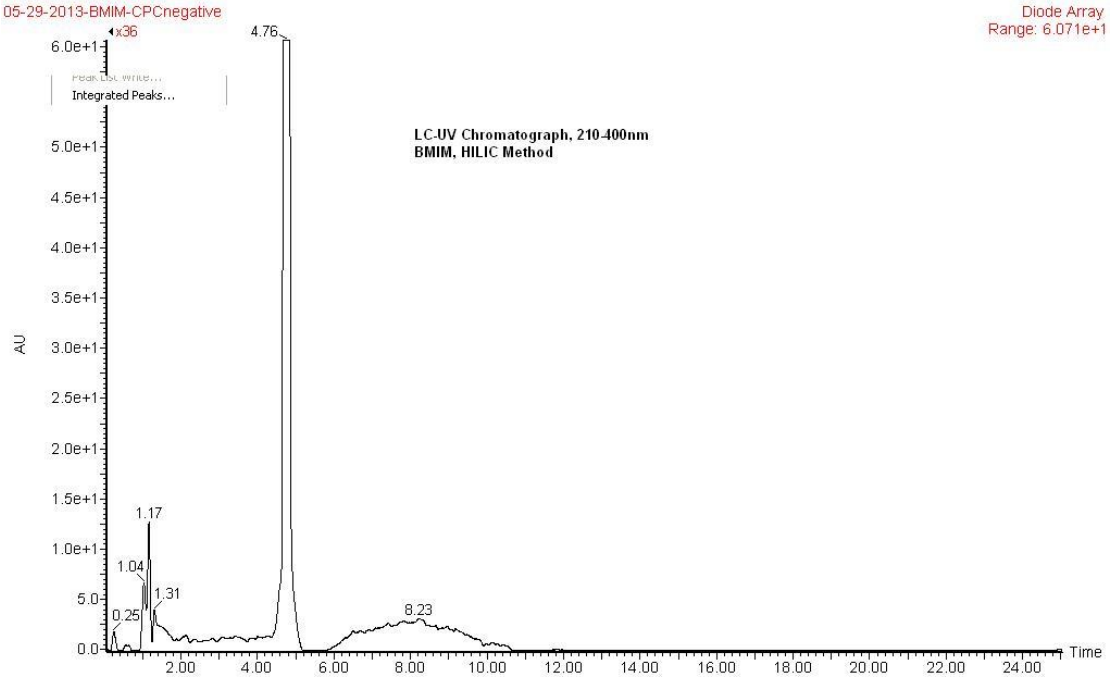

Figure 3.19 LC-UV chromatograph of BMIM at wavelength 210-400nm

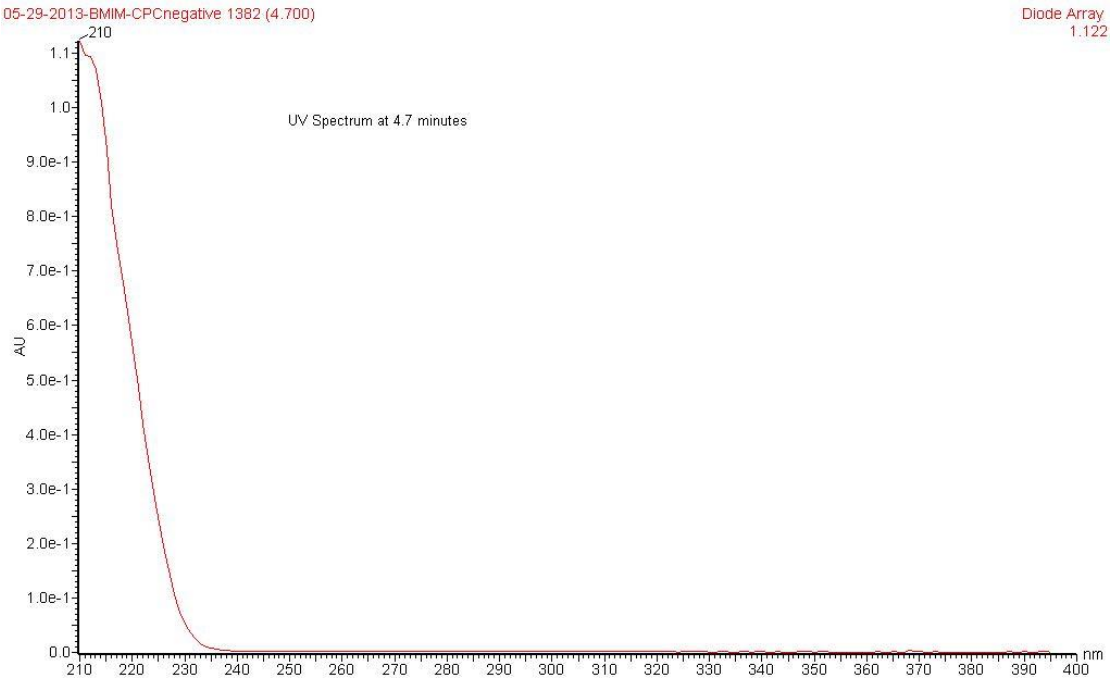

Figure 3.20 UV spectrum at retention time of 4.7 mins for [BMIM][NTf_2]

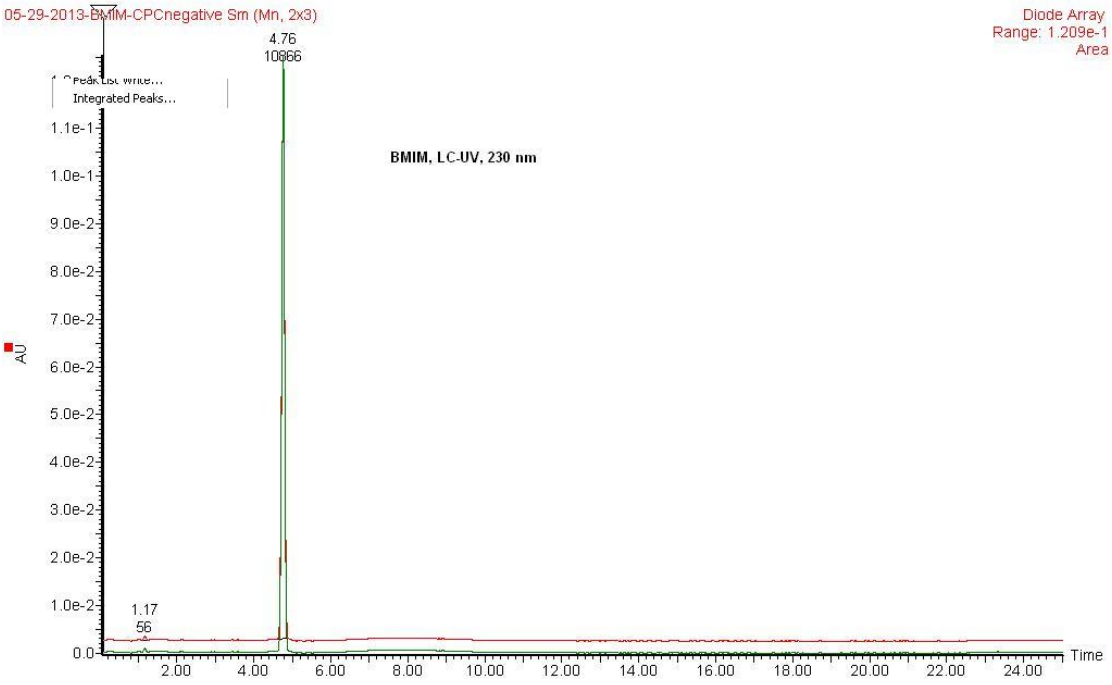

Figure 3.21 LC-UV chromatograph of BMIM at wavelength 230 nm

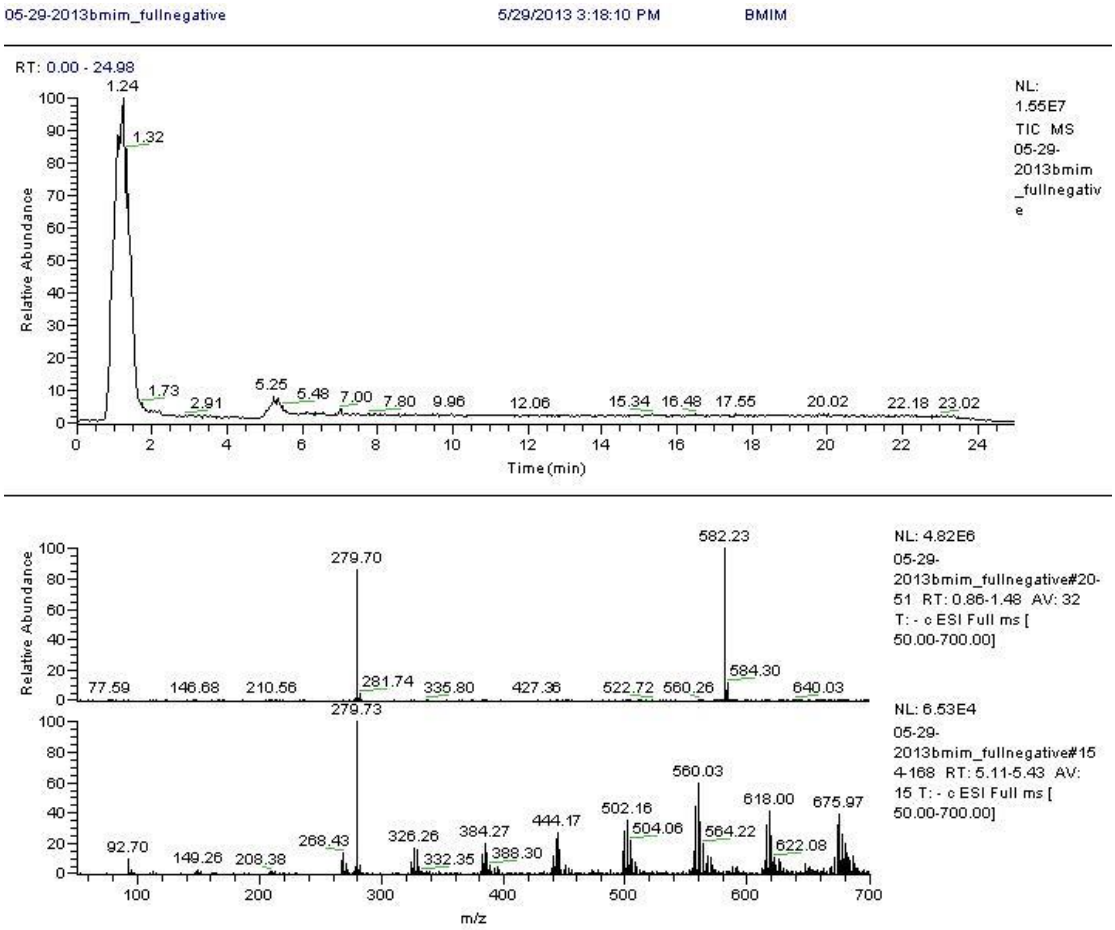

Figure 3.22 LC-UV-MS spectra of [BMIM][NTf_2] on negative mode

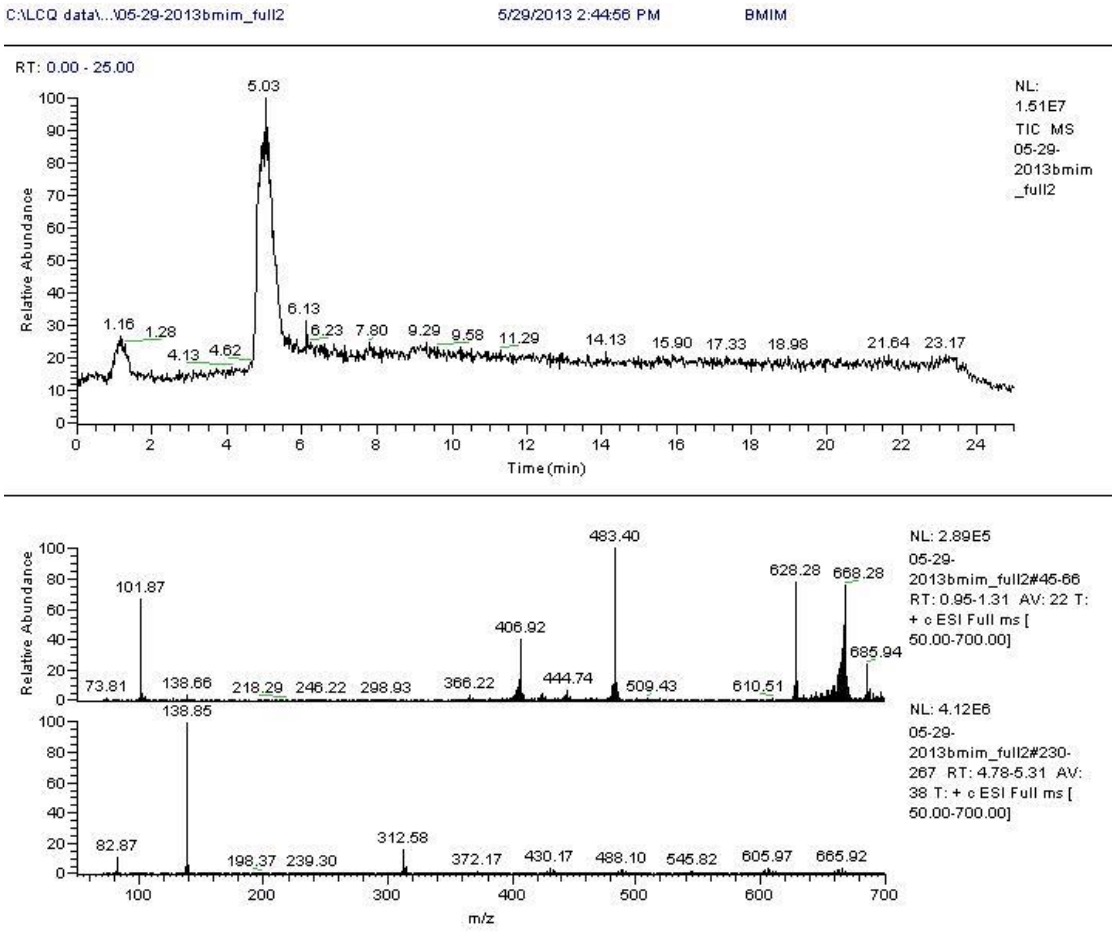

Figure 3.23 LC-UV-MS spectra of [BMIM][NTf_2] on positive mode

From Figure 3.17, 3.18 and 3.19, we could observe that there is an obvious peak around retention time of 4.75 mins, thus we took UV spectrum at retention time of 4.7 mins specifically in figure 3.20, since usually the solvent of acetonitrile has absorption peak at wavelength around 210 nm, so we took LC-UV chromatograph of BMIM at wavelength 230 nm in which a high peak at retention time of 4.76 mins and a tiny peak at retention time of 1.17 mins. After that, we took LC-UV-MS spectra of [BMIM][NTf_2] on negative mode at retention time of 0.86-1.48 mins and 5.11-5.43

mins to comfirm the m/z of those peaks. In the former spectra, there are only two peaks with m/z of 279.7 and 582.2. The peak of 279.7 corresponds to the anion $[NTf_2]^-$ in [BMIM][NTf_2], while peak of 582.2 corresponds to the dimer of $[NTf_2]^-$ plus a sodium cation which might be left inside HPLC from previous tests. As for the positive mode, in figure 3.23, in LC-UV-MS spectra of [BMIM][NTf_2] on positive mode at retention time of 0.95-1.31, there are some random peaks, while in the spectra at retention time of 4.78-5.31, peaks of m/z=138.8 and 312.6 could be observed. The peak of 138.8 refers to cation $[BMIM]^+$ of [BMIM][NTf_2], while the peak of 312.6 should be the dimer of cation plus chloride which might be left inside HPLC from previous tests. In sum, [BMIM][NTf_2] is pretty pure, from the figure 3.21 the LC-UV chromatograph of BMIM at wavelength 230 nm, the integration of peak at 4.76 is 10866 while the integration of peak at 1.17 is 56, thus the purity could be considered as more than 99%. Therefore, there is no need for us to purify this imidazolium-based ionic liquid.

3.4 Conclusion

In this project, we have obtained both calculational and experimental PA for Strassner compounds (TAAILs). Both results demonstrate that TAAILs with electron-withdrawing group do have low ΔH_{acid}, while TAAILs with electron -donating group have higher ΔH_{acid}. Then, we used two methods to measure pK_a of TT1458 in water, giving the value as 25.4 via H/D exchange reaction on NMR. Besides, in order to find relationship between gas phase acidity and pK_a of

imidazolium compounds, we calculated free energy in water for ten imidazolium compounds whose experimental pK_a's have been reported. Then we acquired the calculated pK_a(calc) based on a series of thermodynamic equations, getting a plot of pK_a(exp) vs pK_a(calc) by linear fitting. However, five dots represented by five imidazolium compounds outlie the main trend, which produces a huge derivation. The reason might be from the inaccuracy of calculated free energy in water of those four compounds. At the same time, we also test the purity of [BMIM][NTf_2] for the future work.

3.5 Proposal research

The work needed to be done in the future include conducting H/D exchange reactions on NMR for the other imidazolium-based ionic liquid after examining their purity. NMR parameters may be changed according to the intrinsic property of different imidazolium compounds when they exchange proton with D_2O at various pD. As a suggestion, the interval time of H/D exchange reaction monitored by NMR may vary as the whole system becomes less acidic. For example, for TT1458, we found that as pD getting close to 7, the carbene proton on TT1458 exchanged so rapidly with deuteron in D_2O that there is even no signal of the carbene proton in the beginning of experiment. In this case, it is better for us to shorten the interval time for the last two tests. On the other hand, we can calculate the thermochemical property of all the TAAILs like free energy in solution as well as their calculated pK_a(calc) via mathematics. After getting all the experimental pK_a(exp) values of those TAAILs, we

can plot the graph of pK_a(calc) versus pK_a(exp), finding a linear relationship between them. Or if there was no obviously uniform correlation, we can collect all the imidazolium-based compounds and group them based on substituents to see any correlation among one group of imidazolium compounds. In the meantime, we also need to explore the most accurate method or basis set to calculate the thermochemical property by Gaussian09. By the way, the precipitate in TT1458 solution at pH=13.8 could be extracted via centrifuge techinique and characterized by ^{13}C NMR. If it is the dimer of TT1458 (figure 3.24), this would be an exciting discovery. Since so far there has none report about the existence of this kind dimer, since the unsaturated imidazolium is quite stable, people believe that it would not dimerize under common condition.

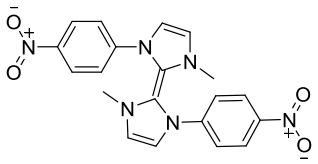

Figure 3.24 Dimer of TT1458

Appendix (NMR data):

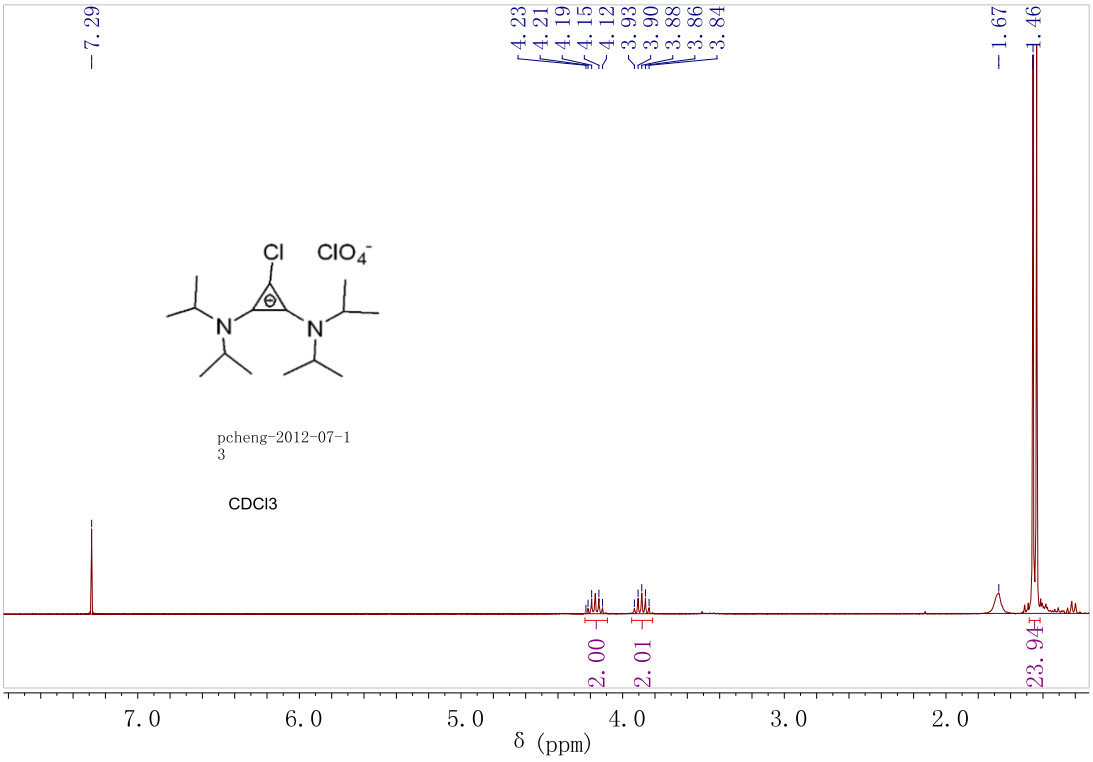

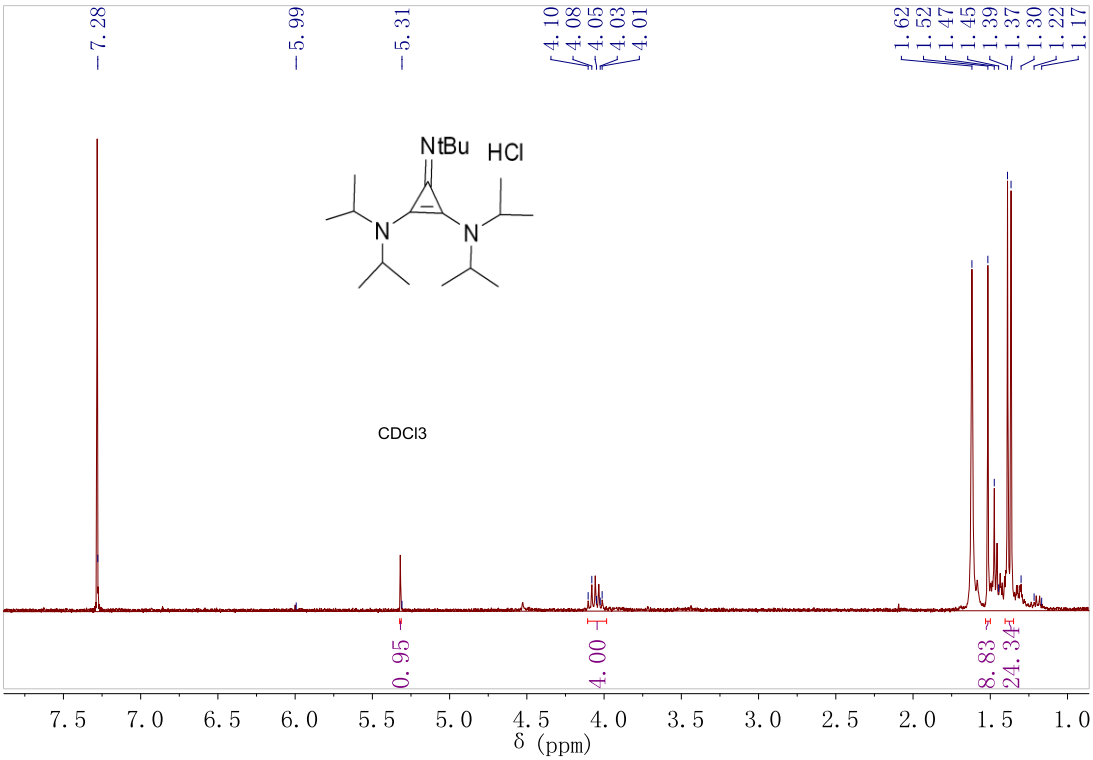

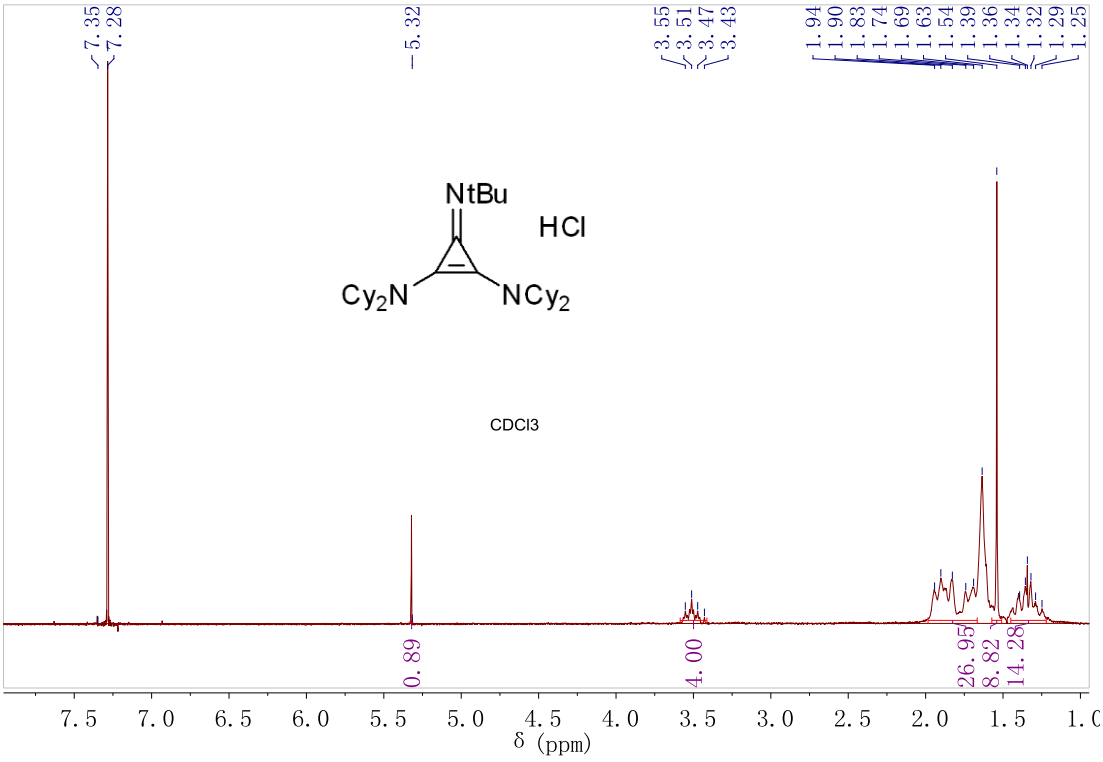
7.35
7.28
5.32
3.55
3.51
3.47
3.43
1.94
1.90
1.83
1.74
1.69
1.63
1.54
1.39
1.36
1.34
1.32
1.29
1.25
NtBu
HCl
Cy2N
NCy2
CDCl3
0.89
4.00
26.95
8.82
14.28
7.5
7.0
6.5
6.0
5.5
5.0
4.5
4.0
3.5
3.0
2.5
2.0
1.5
δ (ppm)

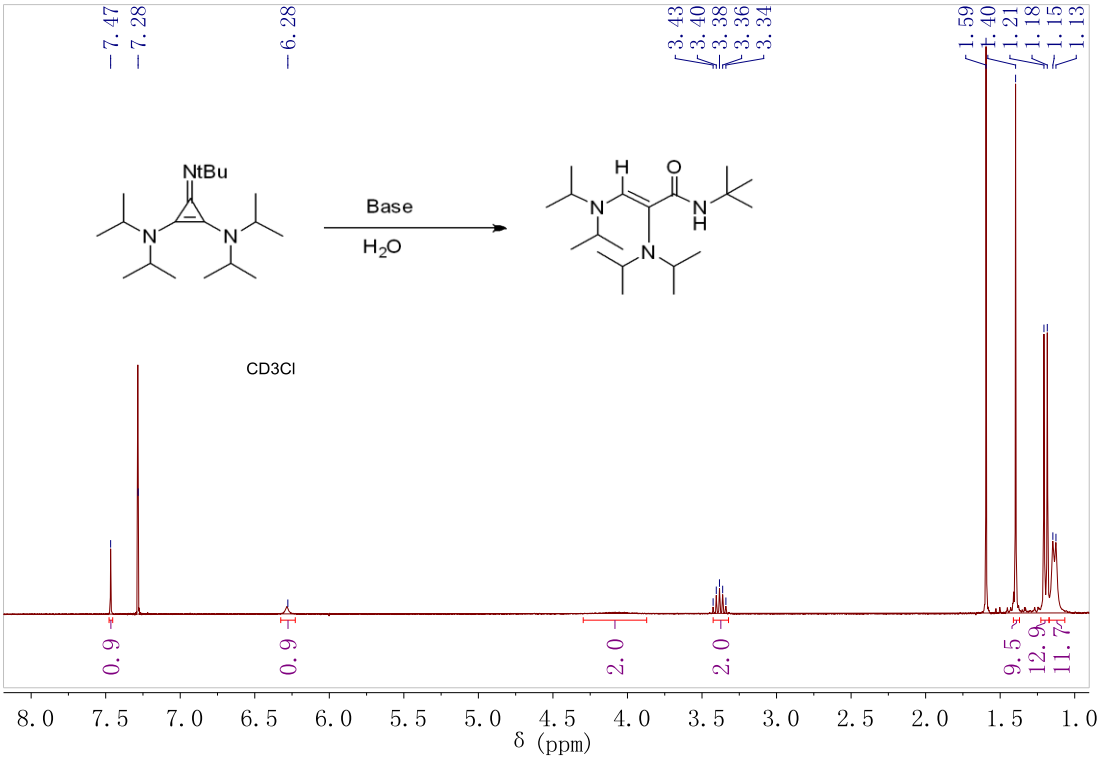
7.47
7.28
6.28
3.43
3.40
3.38
3.36
3.34
1.59
1.40
1.21
1.18
1.15
1.13
NtBu
Base
H2O
H
O
N
N
N
N
H
CD3Cl
0.9
0.9
2.0
2.0
9.5
12.9
11.7
8.0
7.5
7.0
6.5
6.0
5.5
5.0
4.5
4.0
3.5
3.0
2.5
2.0
1.5
1.0
δ (ppm)

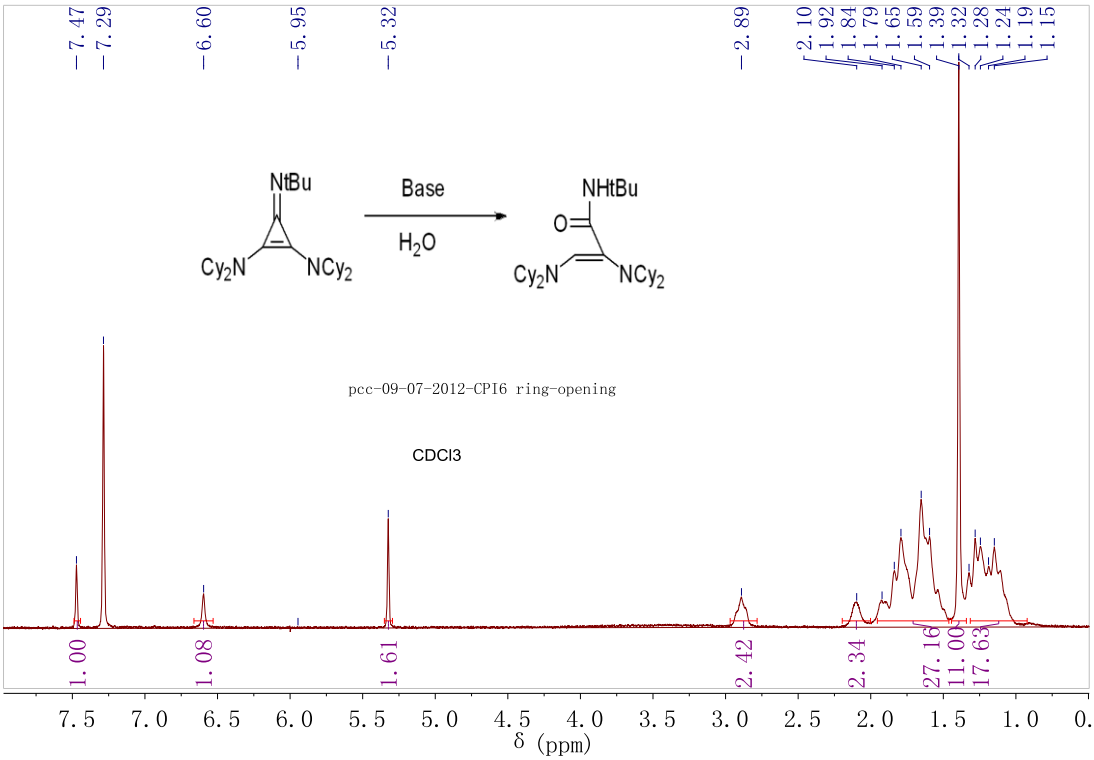
7.47
7.29
6.60
5.95
5.32
2.89
2.10
1.92
1.84
1.79
1.65
1.59
1.39
1.32
1.28
1.24
1.19
1.15
NtBu
Base
H2O
NHtBu
O
Cy2N
NCy2
Cy2N
NCy2
pcc-09-07-2012-CPI6 ring-opening
CDCl3
1.00
1.08
1.61
2.42
2.34
27.16
11.00
17.63
7.5
7.0
6.5
6.0
5.5
5.0
4.5
4.0
3.5
3.0
2.5
2.0
1.5
1.0
0.
δ (ppm)

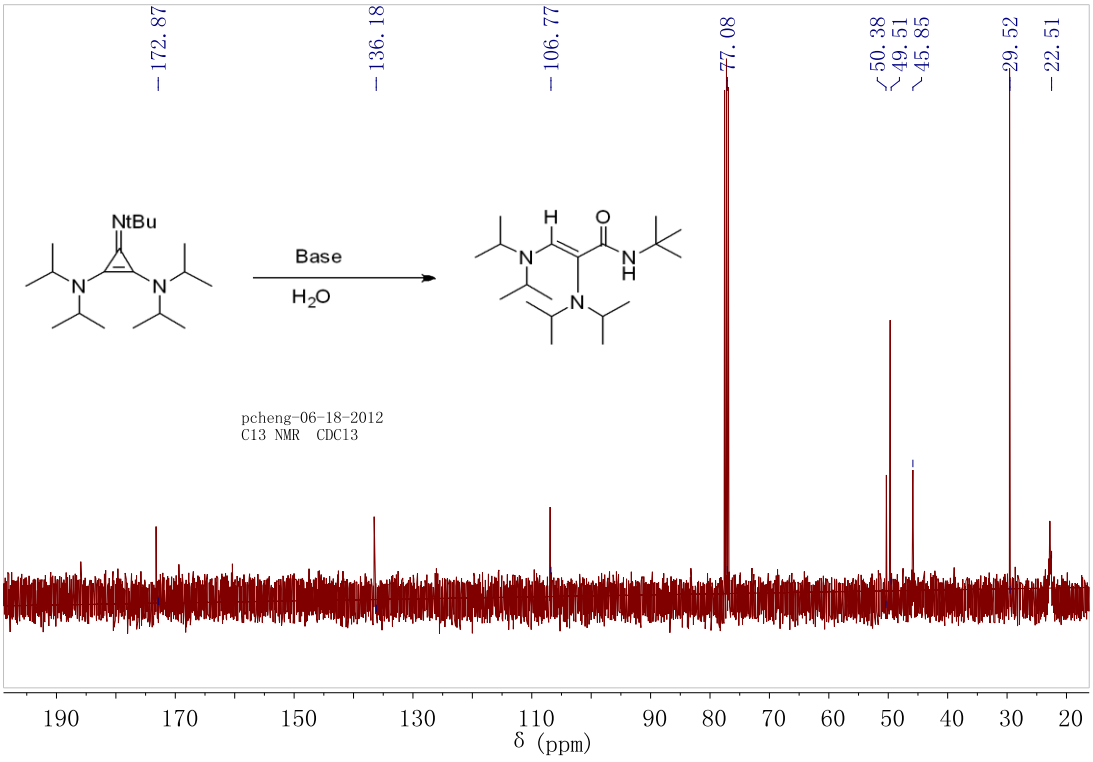
172.87
136.18
106.77
77.08
50.38
49.51
45.85
29.52
22.51
NtBu
N
N
Base
H2O
H
O
N
N
H
pcheng-06-18-2012
C13 NMR CDC13
190
170
150
130
110
90
80
70
60
50
40
30
20
δ (ppm)

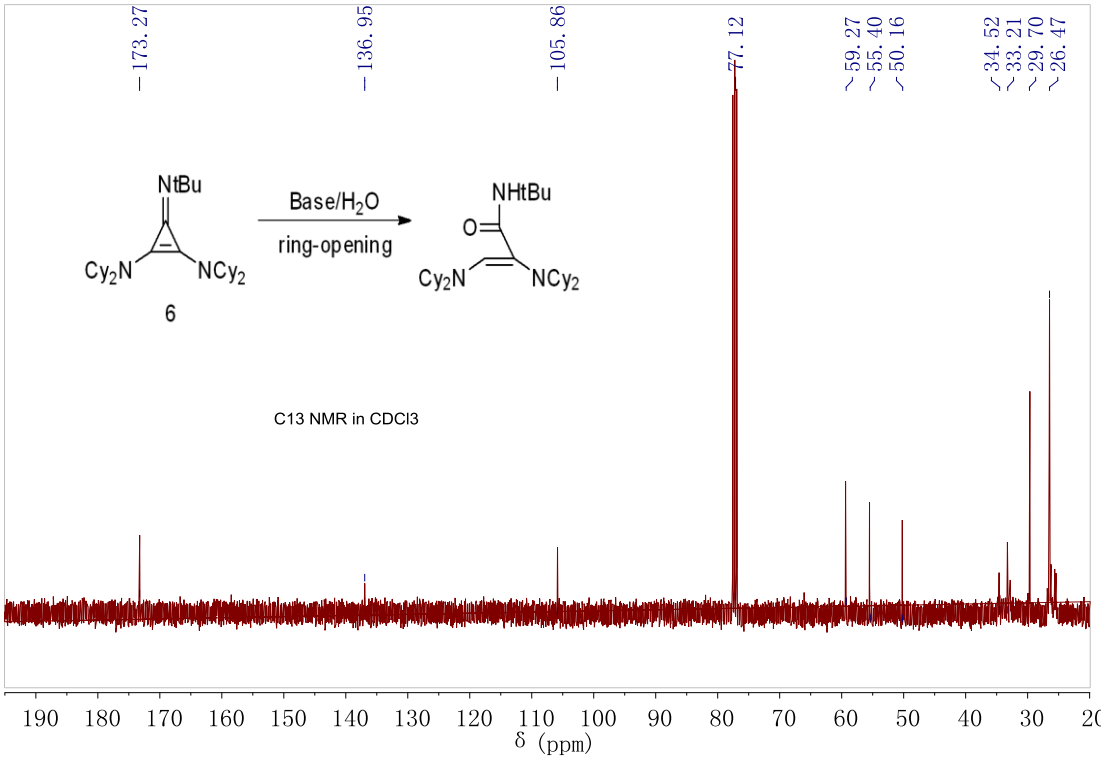
173.27
136.95
105.86
77.12
59.27
55.40
50.16
34.52
33.21
29.70
26.47
NtBu
Base/H2O
ring-opening
NHtBu
O
Cy2N
NCy2
6
C13 NMR in CDCl3
190 180 170 160 150 140 130 120 110 100 90 80 70 60 50 40 30 20
δ (ppm)

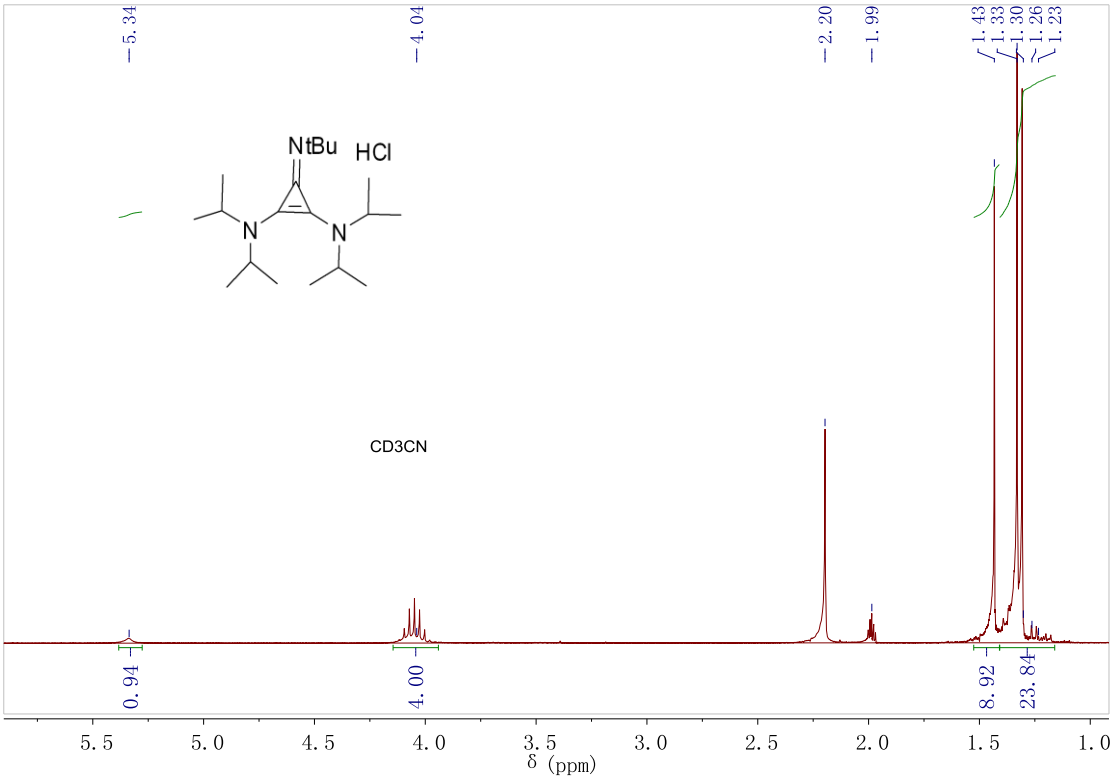
5.34
4.04
2.20
1.99
1.43
1.33
1.30
1.26
1.23
NtBu
HCl
N
N
CD3CN
0.94
4.00
8.92
23.84
5.5 5.0 4.5 4.0 3.5 3.0 2.5 2.0 1.5 1.0
δ (ppm)

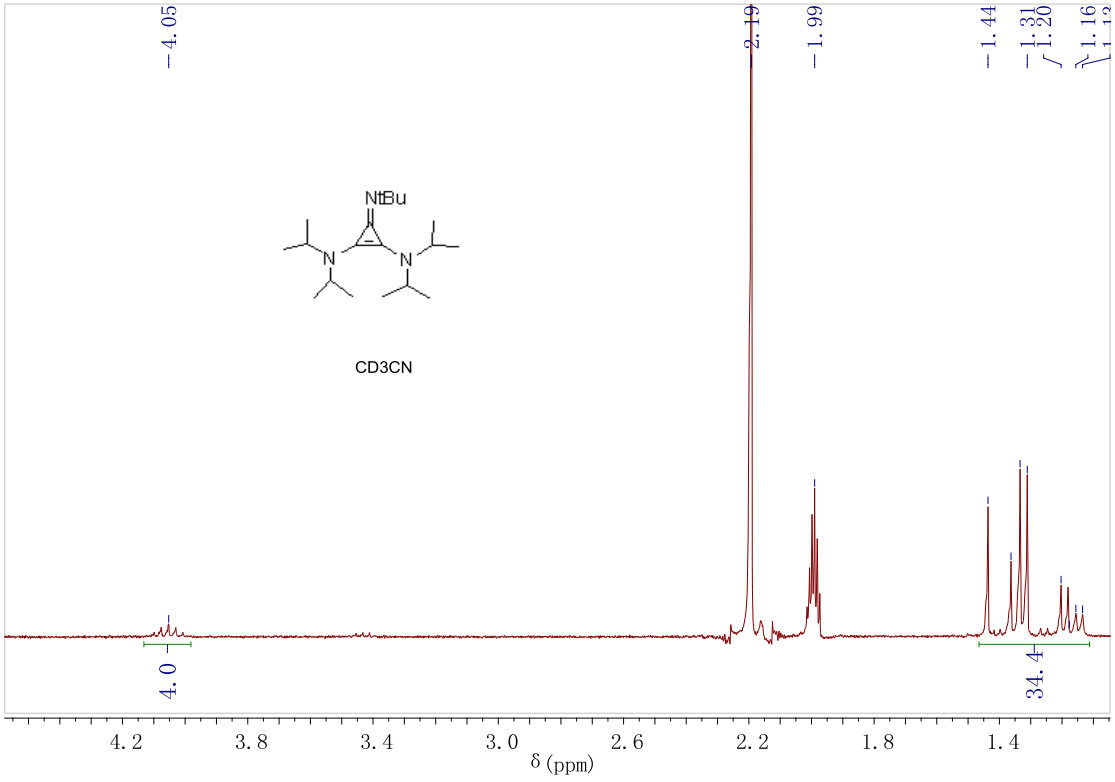
4.05
2.19
1.99
1.44
1.31
1.20
1.16
NtBu
N
N
CD3CN
4.0
34.4
4.2
3.8
3.4
3.0
2.6
2.2
1.8
1.4
δ (ppm)

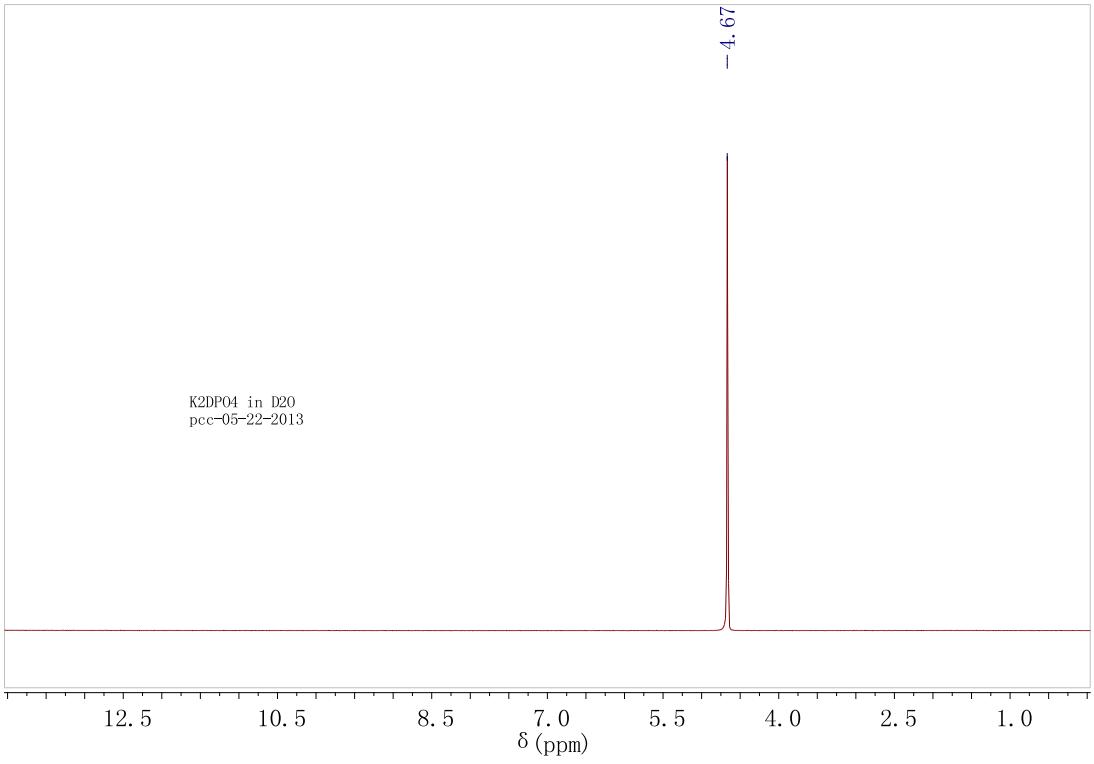
4.67
K2DPO4 in D2O
pcc-05-22-2013
12.5
10.5
8.5
7.0
5.5
4.0
2.5
1.0
δ (ppm)

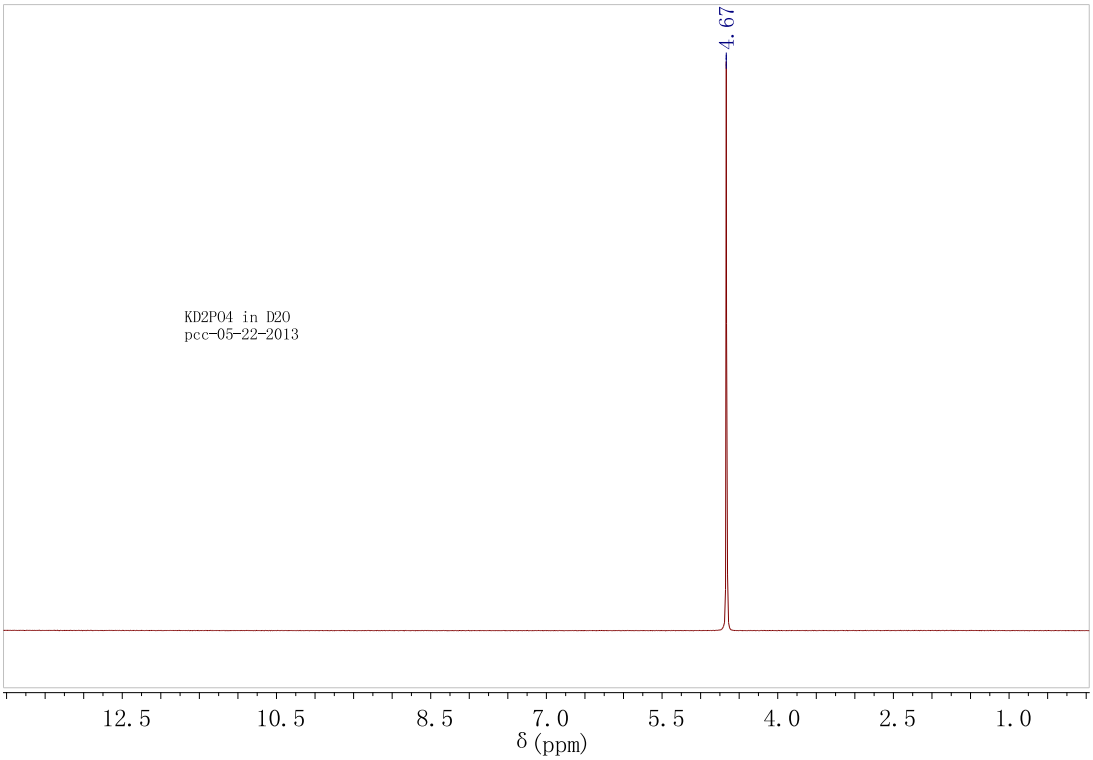
4.67
KD2PO4 in D2O
pcc-05-22-2013
12.5
10.5
8.5
7.0
5.5
4.0
2.5
1.0
δ (ppm)

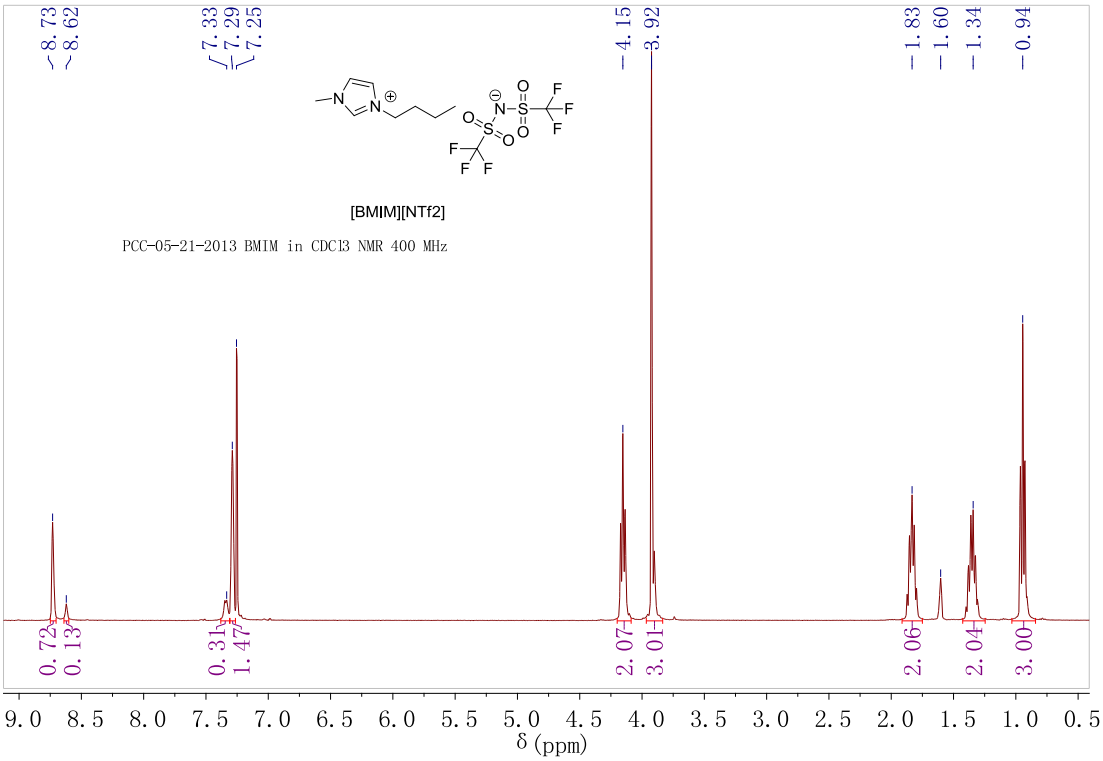
8.73
8.62
7.33
7.29
7.25
4.15
3.92
1.83
1.60
1.34
0.94
[BMIM][NTf2]
PCC-05-21-2013 BMIM in CDCl3 NMR 400 MHz
0.72
0.13
0.31
1.47
2.07
3.01
2.06
2.04
3.00
9.0
8.5
8.0
7.5
7.0
6.5
6.0
5.5
5.0
4.5
4.0
3.5
3.0
2.5
2.0
1.5
1.0
0.5
δ (ppm)

References:

1. De Hoffmann, E., J. Charrette, and V. Stroobant, *Mass Spectrometry Principles and Applications;* John Wiley&Sons, 1999.
2. Linstrom, P.J.M., W. G., Eds., NIST Chemistry WebBook, Nist Standard Reference Database Number 69, June 2005.
3. Oldamur H.; Terleczky, P.S., D.; Mourgas,G.; Gudat, D., J. Am. Chem. Soc., 2011. **133**: p. 780–789.
4. Enders, D., O. Niemeier, and A. Henseler, 2007. **107**(12): p. 5606-5655.
5. Struble, J.R., J. Kaeobamrung, and J.W. Bode, Organic Letters, 2008. **10**(5): p. 957-960.
6. Ahrens, S., A. Peritz, and T. Strassner, Angewandte Chemie-International Edition, 2009. **48**(42): p. 7908-7910.
7. Ferrarello, C.N., et al., *Metal distribution patterns in the mussel Mytilus edulis cytosols using size-exclusion chromatography and double focusing ICP-MS detection.* Analyst, 2000. **125**(12): p. 2223-2229.
8. March, R.E., *Quadrupole Ion Trap Mass Spectrometer.* John Wiley & Sons Ltd: Chichester, 2000.
9. Zhang, S., *Gas phase acidity and proton affinity studies of organic species using mass spectrometry.* Master thesis from Rutgers University.
10. MuLuckey, S. A.; Cameron, D.; Cooks, R. G., *J. Am. Chem. Soc.*, 1981. **103**: p. 1313-1317.
11. Brodbelt-Lustig, J.S.C., R.G. Cooks., Talanta, 1989. **36**: p. 255-260.
12. Green-Church, K.B., Limbach, P. A., *J. Am. Chem. Soc*.Mass Spectrom, 2000. **11**: p. 24-32.
13. Cooks. R.G.; Koskinen. J.T.; Thomas. P.D.; *J. Am. Chem. Soc.*, 1977. **99**.
14. Liu, M., et al., Organic Letters, 2010. **12**(21): p. 4764-4767.
15. M. J. Frisch, G. W. Trucks, H. B. Schlegel et al., *Gaussian03, Rev. C.* Gaussian Inc: Wallingford, CT,, 2004.
16. Cossi, M.; Barone, V.; Cammi, R.; Tomasi, J.; *J. Phys. Chem. A*, 1998. **102**: p. 1995-2001.
17. Cossi, M.; Scalmani, G.; Barone, V., *J. Comput. Chem*, 2003. **24**: p. 669-681.
18. Bandar, J.S.; Lambert. T.H.; *J. Am. Chem. Soc.*, 2012. **134**(12): p. 5552-5555.
19. Maksić. Z.B. and Kovačević.B.; *J. Phys.Chem. A*, 1999. **103**: p. 6678.
20. Z. Gattin, B. Kovačević, Z. B. Maksić,, Eur. *J. Org. Chem.*, 2005: p. 3206.
21. Kaljurand, L. Soovali, T. Rodima, V. Mäemets, I. Leito.; *J. Org. Chem.* , 2005. **70**: p. 1019.
22. Trnka, T. M.; Grubbs, R. H., *Acc. Chem. Res.*, 2001. **34**: p. 18-29.
23. Marion, N.; Nolan, S. P.; Acc. *Chem. Res.*, 2008. **41**: p. 1440–1449.
24. Tekavec.T.N.; J. Louie.; *Top.Organomet. Chem.*, 2007. **21**: p. 159–192.
25. Palomo, C., M. Oiarbide, and R. Lopez, *Chemical Society Reviews*, 2009. **38**(2): p. 632-653.

26. Schwesinger, R. and H. Schlemper, Angewandte Chemie-International Edition in English, 1987. **26**(11): p. 1167-1169.
27. Raczynska, E.D., et al., *Journal of Physical Organic Chemistry*, 1994. **7**(12): p. 725-733.
28. Breslow, R.; Yuan, C., *J. Am. Chem. Soc*, 1958. **80**: p. 5991.
29. Breslow, R., J. Am. Chem. Soc., 1957. **79**: p. 5318.
30. Komatsu, K.; Kitagawa, T.; *Chem. Rev.*, 2003. **103**: p. 1371.
31. Amyes, T.L., et al., *J. Am. Chem Soc*, 2004. **126**(13): p. 4366-4374.
32. A.M. Magill, K.J. Cavell, B.F. Yates.; *J. Am. Chem. Soc*, 2004. **126**(28): p. 8717-8724.
33. Bruns, H., et al., Angewandte Chemie-International Edition, 2010. **49**(21): p. 3680-3683.
34. Lindsay, A., Geraldine, *Mechanism-Guided Studies of Brønsted Acid and Base Organocatalysis,*. PhD thesis from Durham University.
35. Bohm, V.P.W., et al., *Angewandte Chemie-International Edition*, 2000. **39**(9): p. 1602-.
36. Sauers, R.R., Tetrahedron Letters, 1996. **37**(43): p. 7679-7682.
37. Kim, Y.J. and A. Streitwieser, J. Am. Chem. Soc., 2002. **124**(20): p. 5757-5761.
38. Alder, R.W., P.R. Allen, and S.J. Williams, *Journal of the Chemical Society-Chemical Communications*, 1995(12): p. 1267-1268.
39. Rios, A., T.L. Amyes, and J.P. Richard, *J. Am. Chem. Soc*, 2000. **122**(39): p. 9373-9385.
40. Rios, A., et al., *J. Am. Chem. Soc.*, 2001. **123**(32): p. 7949-7950.
41. Richard, J.P., T.L. Amyes, and M.M. Toteva, *Accounts of Chemical Research*, 2001. **34**(12): p. 981-988.
42. Richard, J.P., et al., *J. Am. Chem. Soc*., 2002. **124**(12): p. 2957-2968.
43. Kaatze, U., *J. Chem and Eng Data*, 1989. **34**(4): p. 371-374.
44. Richard, J.P., K.B. Williams, and T.L. Amyes, *J. Am. Chem. Soc.*, 1999. **121**(36): p. 8403-8404.
45. Bednar, R.A. and W.P. Jencks, *J. Am. Chem. Soc.*, 1985. **107**(24): p. 7135-7138.
46. Herrmann, W.A.K.c., C, *Angew. Chem., Int. Ed. Engl*, 1997. **36**: p. 2162-2187.
47. Ogretir, C., et al., *J. Molecular Structure-Theochem*, 2006. **759**(1-3): p. 73-78.

CURRICULUM VITAE

Pingcheng Chu

Education:

2007-2011	B.S., Chemistry, Polymer Science University of Science and technology of China, P.R.China
2011-2013	M.S., Chemistry and Chemical Biology Rutgers, the State University of New Jersey